AD-A110 096 AIR FORCE INST OF TECH WRIGHT-PATTERSON AFB OH F/G 20/11
A PLANE STRAIN PLASTICITY ANALYSIS OF THE ANCHOR PULLOUT PROBLE--ETC(U)
1981 H F KELLY
UNCLASSIFIED AFIT-CI-81-65T NL

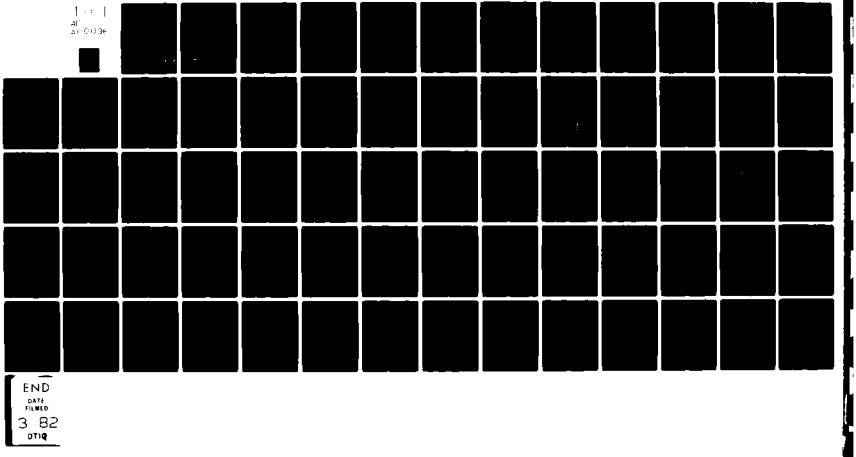

END
DATE FILMED
3 82
DTIC

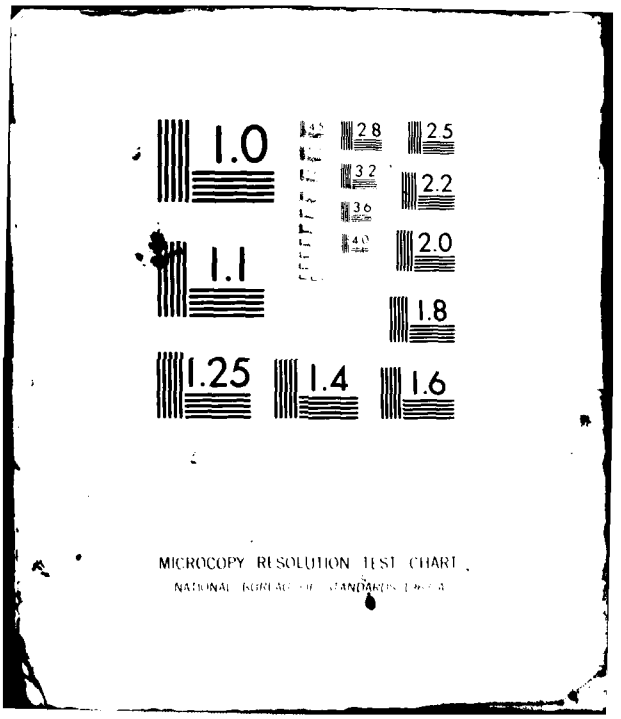
1.0
1.1
1.25
1.4
1.6
1.8
2.0
2.2
2.5
2.8
3.2
3.6
4.0
MICROCOPY RESOLUTION TEST CHART

A PLANE STRAIN PLASTICITY ANALYSIS OF THE ANCHOR PULLOUT PROBLEM

by

Henry Francis Kelly

A Thesis Submitted to the Faculty of the

DEPARTMENT OF CIVIL ENGINEERING AND ENGINEERING MECHANICS

In Partial Fulfillment of the Requirements
For the Degree of

MASTER OF SCIENCE

In the Graduate College

THE UNIVERSITY OF ARIZONA

1 9 8 1

UNCLASS

SECURITY CLASSIFICATION OF THIS PAGE (When Data Entered)

REPORT DOCUMENTATION PAGE		READ INSTRUCTIONS BEFORE COMPLETING FORM
1. REPORT NUMBER 81-65T	2. GOVT ACCESSION NO. AD-A110 096	3. RECIPIENT'S CATALOG NUMBER
4. TITLE (and Subtitle) A Plane Strain Plasticity Analysis of the Anchor Pullout Problem		5. TYPE OF REPORT & PERIOD COVERED THESIS/DISSERTATION 6. PERFORMING ORG. REPORT NUMBER
7. AUTHOR(s) Henry Francis Kelly		8. CONTRACT OR GRANT NUMBER(s)
9. PERFORMING ORGANIZATION NAME AND ADDRESS AFIT STUDENT AT: University of Arizona		10. PROGRAM ELEMENT, PROJECT, TASK AREA & WORK UNIT NUMBERS
11. CONTROLLING OFFICE NAME AND ADDRESS AFIT/NR WPAFB OH 45433		12. REPORT DATE 1981 13. NUMBER OF PAGES 58
14. MONITORING AGENCY NAME & ADDRESS(if different from Controlling Office)		15. SECURITY CLASS. (of this report) UNCLASS 15a. DECLASSIFICATION/DOWNGRADING SCHEDULE

16. DISTRIBUTION STATEMENT (of this Report)

APPROVED FOR PUBLIC RELEASE; DISTRIBUTION UNLIMITED

17. DISTRIBUTION STATEMENT (of the abstract entered in Block 20, if different from Report)

APPROVED FOR PUBLIC RELEASE AFR 190 17.

22 JAN 1982

FREDRIC C. LYNCH, Major, USAF
Director of Public Affairs
Air Force Institute of Technology (ATC)
Wright-Patterson AFB, OH 45433

18. SUPPLEMENTARY NOTES

APPROVED FOR PUBLIC RELEASE: IAW AFR 190-17

19. KEY WORDS (Continue on reverse side if necessary and identify by block number)

20. ABSTRACT (Continue on reverse side if necessary and identify by block number)

[redacted]

DTIC COPY INSPECTED

Accession For	
NTIS GRA&I	X
DTIC TAB	☐
Unannounced	☐
Justification	
By	
Distribution/	
Availability Codes	
Dist	Avail and/or Special
A	

DD FORM 1 JAN 73 1473 EDITION OF 1 NOV 65 IS OBSOLETE

UNCLASS

SECURITY CLASSIFICATION OF THIS PAGE (When Data Entered)

82 02 01 080

STATEMENT BY AUTHOR

This thesis has been submitted in partial fulfillment of requirements for an advanced degree at The University of Arizona and is deposited in the University Library to be made available to borrowers under rules of the Library.

Brief quotations from this thesis are allowable without special permission, provided that accurate acknowledgment of source is made. Requests for permission for extended quotation from or reproduction of this manuscript in whole or in part may be granted by the head of the major department or the Dean of the Graduate College when in his judgment the proposed use of the material is in the interests of scholarship. In all other instances, however, permission must be obtained from the author.

SIGNED: Henry F. Kelly

APPROVAL BY THESIS DIRECTOR

This thesis has been approved on the date shown below:

E. A. NOWATZKI
Associate Professor, Civil Engineering
and Engineering Mechanics

Date

ACKNOWLEDGMENTS

I wish to express my gratitude and appreciation to Professor Edward A. Nowatzki, who, throughout the course of this research, contributed so much in the way of guidance, time, and knowledge. I am also thankful to Professors Hassan A. Sultan and Ralph M. Richard for the help they have given me.

I especially wish to express my sincere appreciation to my dear wife, Gale, for her patience, support and encouragement throughout this study program.

TABLE OF CONTENTS

TABLE OF CONTENTS -- Continued

LIST OF ILLUSTRATIONS

LIST OF TABLES

ABSTRACT

The purpose of this thesis is to analyze the vertical pullout capacity of a horizontal circular anchor plate embedded in soil, using the plasticity theory as developed by Sokolovskii (1960).

A mathematical model for soil-structure interaction was used to generate slip line fields compatible with the boundary conditions of the anchor pullout problem. To see if the solution for a given set of boundary conditions was physically admissible, computer-generated plots of slip line fields were obtained. If the slip line field was permissible, i.e., no overlapping of characteristic lines. The pullout capacity was then calculated. A conventional Coulomb sliding wedge graphical solution was performed. The results of the hand solution closely approximate the computer results.

The theoretically determined pullout capacities were found to be less than experimental results of others. In loose sand, at small depth to anchor plate diameter (D/B) ratios, the predicted values were approximately 81 percent of experimental results, while in dense sand they were approximately 50 percent of experimental results.

CHAPTER 1

INTRODUCTION

The purpose of this thesis is to study the anchor pullout problem using the theory of plasticity and the Coulomb failure criteria for soils in the analysis.

The Problem

The problem is to determine the pullout capacity of a circular plate embedded below a horizontal ground surface and centrally loaded by an upward vertical force. Pullout capacity is defined as the maximum vertical load or pull required to remove the anchor from the soil.

Earth anchors are used to provide uplift resistance for transmission towers, submerged pipelines and tunnels, mobile homes, aircraft and ocean mooring systems, and to develop tieback forces required to eliminate external bracing from retaining structures and sheeting walls.

Previous anchor pullout determinations are based on semi-empirical methods and/or theoretical methods that make some limiting assumptions. Therefore, there is a need for study to find a reliable method of determining the anchor pullout capacity.

Scope

This thesis presents a theoretical, computer determination of the pullout capacity and associated slip line field for anchors having various depth of embedment to anchor diameter (D/B) ratios, for both loose and dense sand. A description of the theory applicable to the problem is presented first, followed by a literature review of anchor pullout studies, the solution procedure, a presentation and discussion of results, and finally, conclusions and recommendations for future studies.

CHAPTER 2

PLASTICITY THEORY APPLICABLE TO PROBLEM

The initial applications of the plasticity theory were mainly in the field of metallurgy. Calculations based on limiting stress fields for soils were first reported in detail by Sokolovskii (1960 and 1965). He used the method of characteristics to derive the stress fields for materials possessing cohesion or friction or both. It is Sokolovskii's method, as outlined by Harr (1966) and Karafiath and Nowatzki (1978) that was used in this study. To understand the author's solution procedure better, a brief description of Sokolovskii's method is presented in this chapter.

Fundamental to analyses by plasticity theory is the assumption that the soil acts as a rigid-perfectly plastic material. This means that under load, the soil behaves as illustrated by the solid line in Figure 1. The material does not deform, regardless of loading sequence, stress history, rate of loading, etc., until it reaches failure. This differs from elastic-plastic material behavior illustrated by the dashed line in Figure 1. Here the soil undergoes recoverable deformation before reaching failure. In

both cases, deformation at failure takes place at a constant rate without change in stress.

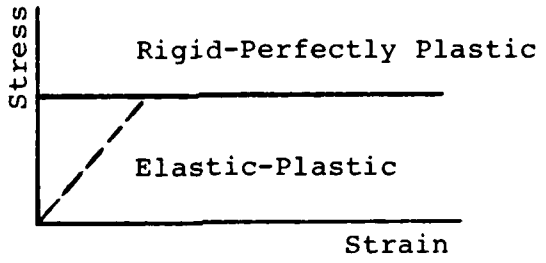

Figure 1. Material behavior (after Karafiath and Nowatzki, 1978).

Fundamental Concepts and Relationships

The stress condition at a point, A, within a semi-infinite homogeneous soil mass under a state of loading, with horizontal x-axis and vertical z-axis, is shown in Figure 2. Lines OF and OF' are the Mohr-Coulomb strength envelopes. The directions of the lines of impending rupture, called slip lines, are indicated by the angles μ which are measured + and - from the direction of the major principal stress, and which can be expressed as:

$$\mu = \pi/4 - \phi/2 \qquad (1)$$

The orientation of the major principal stress with respect to the horizontal is given by the angle θ. If the x-axis is taken along the horizontal, then θ is the angle between

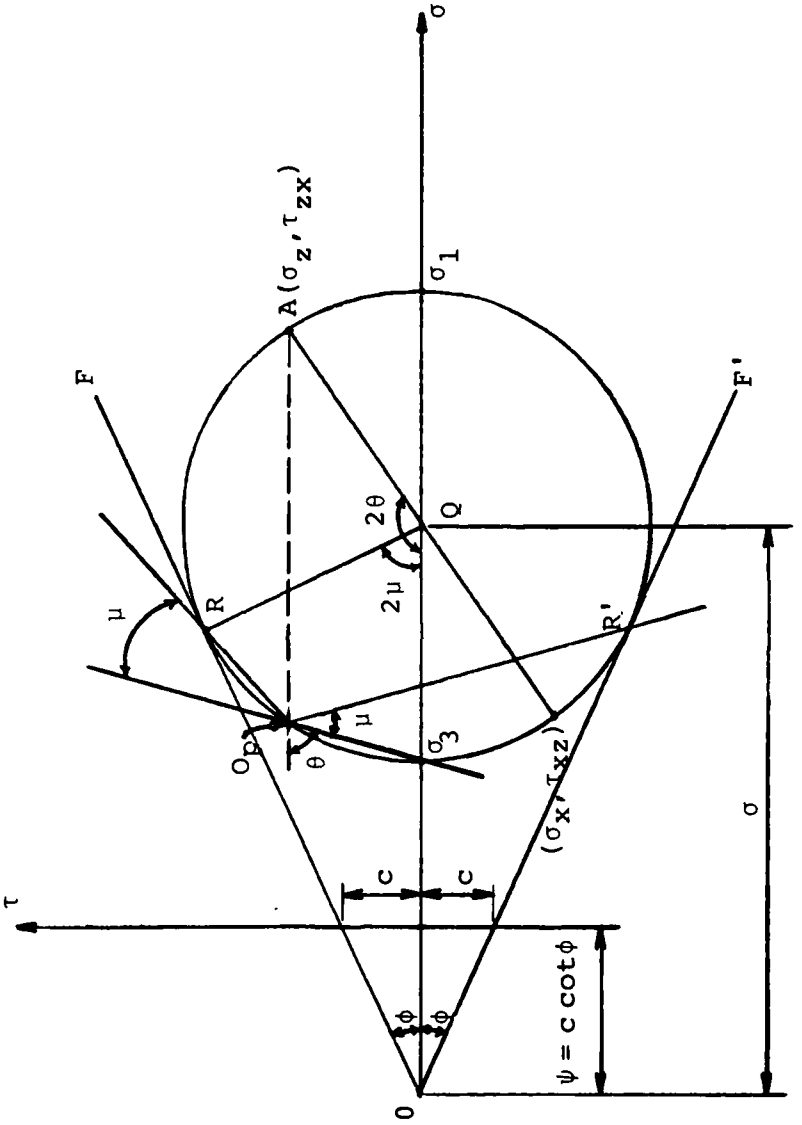

Figure 2. Mohr-Coulomb circle (after Harr, 1966).

the direction of the major principal stress and the x-axis. The symbol σ (without subscript) is used to indicate the stress magnitude on the τ-σ axis from 0, the point of intersection of the Mohr-Coulomb envelope and the σ-axis, to the center of the Mohr circle, Q. In general, $\sigma = (\sigma_x + \sigma_z)/2 + \psi$, where $\psi = c \cot \phi$. Therefore, the stress state at any point can be expressed as:

$$\sigma_x = \sigma(1 + \sin \phi \cos 2\theta) - \psi$$

$$\sigma_z = \sigma(1 - \sin \phi \cos 2\theta) - \psi \qquad (2)$$

$$\tau_{xz} = \sigma \sin \phi \sin 2\theta$$

Figure 3 shows the convention used to describe the orientation of the various stresses discussed above for the point in question. This figure demonstrates that the slip lines at any point can be written in differential form as:

$$\frac{dz}{dx} = \tan (\theta \pm \mu) \qquad (3)$$

The $\mu(+)$ sign refers to "i-characteristic" slip lines inclined at a slope of $\tan (\theta + \mu)$ from the x-axis and the $\mu(-)$ sign refers to "j-characteristic" slip lines inclined at a slope of $\tan (\theta - \mu)$ from the x-axis. The term "slip line field" is understood to mean the two families of curves defining the bounds of regions in which stress states correspond to those of incipient plastic failure. The

directions correspond to the directions of shearing stress causing the failure.

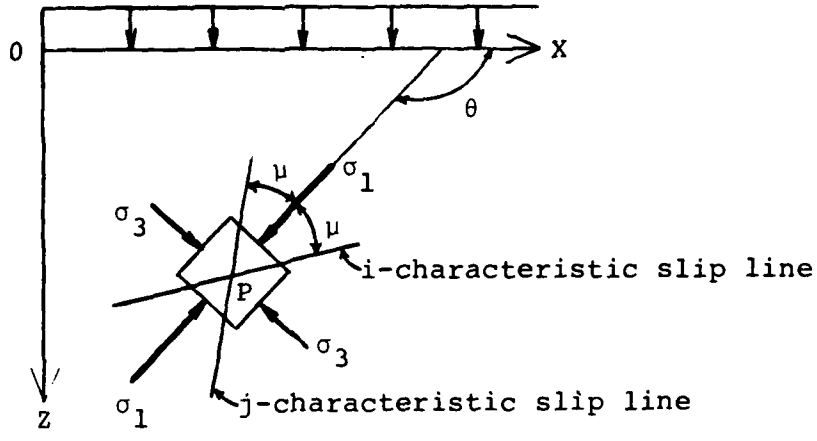

Figure 3. Orientations (after Karafiath and Nowatzki, 1978).

Assuming that the x-axis is not horizontal but is inclined at an angle ε to the direction of gravity, and assuming that inertia and seepage forces are zero, the normal and shear stresses σ_x, σ_z, τ_{xz} on any soil element must satisfy the static equilibrium equations:

$$\frac{\partial \sigma_x}{\partial x} + \frac{\partial \tau_{xz}}{\partial z} = \gamma \sin \varepsilon$$

$$\frac{\partial \sigma_z}{\partial z} + \frac{\partial \tau_{xz}}{\partial x} = \gamma \cos \varepsilon \qquad (4)$$

where γ = effective unit weight.

Substituting Equations 2 into Equations 4 yields the basic differential equation of plastic equilibrium for soil

under plane stress conditions. Sokolovskii modified these equations to yield:

$$d\sigma \pm 2\sigma \tan\phi \, d\theta = \frac{\gamma}{\cos\phi} [\sin(\varepsilon \pm \phi) dx + \cos(\varepsilon \pm \phi) dz] \tag{5}$$

Numerical Solution

Numerical methods are required for solution of Equations 3 and 5, for cases of practical interest. Assuming that the x-axis is horizontal, i.e., $\varepsilon = 0$, the equations become:

For i-characteristics (the slip lines corresponding to i = constant):

$$dz = dx \tan(\theta + \mu) \tag{6a}$$

$$d\sigma + 2\sigma \tan\phi \, d\theta = \gamma(dz + \tan\phi dx) \tag{6b}$$

For j-characteristics (the slip lines corresponding to j = constant):

$$dz = dx \tan(\theta - \mu) \tag{6c}$$

$$d\sigma - 2\sigma \tan\phi \, d\theta = \gamma(dz - \tan\phi dx) \tag{6d}$$

All points in the i-j coordinate system of Figure 4a can be assigned a position in terms of a nodal number $\lambda_{i,j}$ where the i denotes the abscissal reference and j the ordinate. Associated with every nodal point $\lambda_{i,j}$ are the quantities $x_{i,j}$, $z_{i,j}$, $\sigma_{i,j}$, and $\theta_{i,j}$. All nodal points in

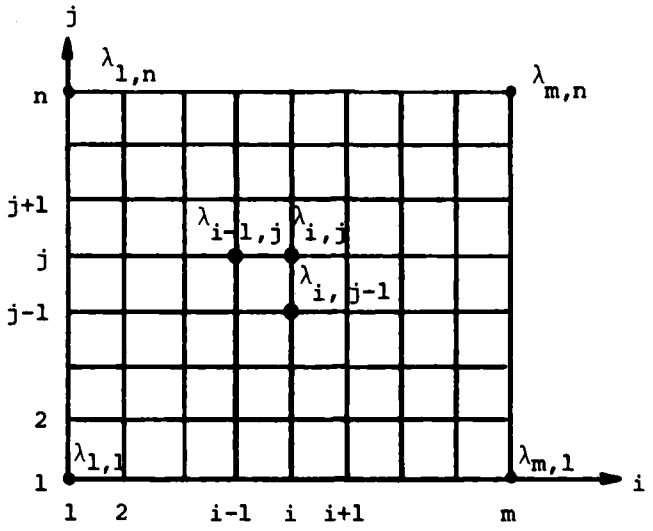

(a)

i / j	1	2		i-1	i		m
1	$x_{1,1}$ $z_{1,1}$ $\sigma_{1,1}$ $\theta_{1,1}$						$x_{m,1}$ $z_{m,1}$ $\sigma_{m,1}$ $\theta_{m,1}$
2							
j-1					$x_{i,j-1}$ $z_{i,j-1}$ $\sigma_{i,j-1}$ $\theta_{i,j-1}$		
j				$x_{i-1,j}$ $z_{i-1,j}$ $\sigma_{i-1,j}$ $\theta_{i-1,j}$	$x_{i,j}$ $z_{i,j}$ $\sigma_{i,j}$ $\theta_{i,j}$		
n	$x_{1,n}$ $z_{1,n}$ $\sigma_{1,n}$ $\theta_{1,n}$						$x_{m,n}$ $z_{m,n}$ $\sigma_{m,n}$ $\theta_{m,n}$

(b)

Figure 4. Characteristics (after Harr, 1966).

grid (Figure 4a) and all pertinent information relative to each point can be put into tabular form (Figure 4b). The basic problem is to determine the values of x, z, σ, and θ at nodal points of interest from known values of these parameters at neighboring nodal points.

To solve Equations 6, Sokolovskii used a finite-difference procedure, and proposed that they be replaced by finite equivalents as follows:

Along i-characteristics:

$$(z_{i,j} - z_{i,j-1}) = (x_{i,j} - x_{i,j-1}) \tan (\theta_{i,j-1} + \mu) \tag{7a}$$

$$(\sigma_{i,j} - \sigma_{i,j-1}) + 2\sigma_{i,j-1}(\theta_{i,j} - \theta_{i,j-1}) \tan\phi = \gamma[(z_{i,j} - z_{i,j-1}) + (x_{i,j} - x_{i,j-1}) \tan\phi] \tag{7b}$$

Along j-characteristics:

$$(z_{i,j} - z_{i-1,j}) = (x_{i,j} - x_{i-1,j}) \tan (\theta_{i-1,j} - \mu) \tag{7c}$$

$$(\sigma_{i,j} - \sigma_{i-1,j}) - 2\sigma_{i-1,j} (\theta_{i,j} - \theta_{i-1,j}) \tan\phi = \gamma[(z_{i,j} - z_{i-1,j}) - (x_{i,j} - x_{i-1,j}) \tan\phi] \tag{7d}$$

Equations 7 represent four equations in four unknowns. Solving these equations results in the following recurrence formulas:

$$x_{i,j} = \frac{z_{i-1,j} - z_{i,j-1} + x_{i,j-1}\tan(\theta_{i,j-1}+\mu) - x_{i-1,j}\tan(\theta_{i-1,j}-\mu)}{\tan(\theta_{i,j-1}+\mu) - \tan(\theta_{i-1,j}-\mu)} \tag{8a}$$

$$z_{i,j} = z_{i-1,j} + (x_{i,j} - x_{i-1,j}) \tan(\theta_{i-1,j} - \mu) \tag{8b}$$

$$\sigma_{i,j} = \frac{\gamma(C\sigma_{i,j-1} + D\sigma_{i-1,j}) + 2\sigma_{i,j-1}\sigma_{i-1,j}[1 + (\theta_{i,j-1} - \theta_{i-1,j})\tan\phi]}{\sigma_{i,j-1} + \sigma_{i-1,j}} \tag{8c}$$

where

$$C = (z_{i,j} - z_{i-1,j}) - \tan\phi\,(x_{i,j} - x_{i-1,j})$$

$$D = (z_{i,j} - z_{i,j-1}) + \tan\phi\,(x_{i,j} - x_{i,j-1})$$

$$\theta_{i,j} = \frac{\sigma_{i,j-1} - \sigma_{i-1,j} + 2\tan\phi(\sigma_{i,j-1}\theta_{i,j-1} + \sigma_{i-1,j}\theta_{i-1,j}) + \gamma(D-C)}{2\tan\phi\,(\sigma_{i,j-1} + \sigma_{i-1,j})} \tag{8d}$$

Equations 8 demonstrate that the quantities x, z, σ, and θ can be determined at a node $\lambda_{i,j}$ if and only if they are known at the two nodes $\lambda_{i,j-1}$ and $\lambda_{i-1,j}$ in the near vicinity of the node. However, the values of all the variables are not always known on a given boundary, nor are boundaries always coincident with characteristic lines. Basically, three types of boundary-value problems are encountered: the Cauchy problem, the Goursat problem, and the Mixed Boundary-Value problem.

Cauchy Problem

In this problem (Figures 5a and 5b), x, z, σ, and θ are known at all points on a non-characteristic line, such as AB, along which neither i nor j is constant. The problem is to determine these variables along characteristic lines within and on other boundaries of the triangle ABC. To accomplish this, AB is first divided conveniently into n sections by introducing the i and j characteristics as shown in Figure 4. Then the values of x, z, σ, and θ at each node represented by the intersection of the characteristics with AB are recorded in the appropriate squares of the table given in Figure 5b. These values occupy the diagonal spaces shown shaded in the figure. The recurrence relations (Equations 8) are used to determine the desired values. Proceeding in an orderly manner according to the arrows shown in the figure, the entire region can be filled and the quantities extended to the boundaries of the triangle.

Goursat Problem

For this problem (Figures 5c and 5d), the quantities x, z, σ, and θ are known at all points on the characteristics AB and AC. As with the Cauchy problem, the Goursat problem is solved by proceeding from two known points to an unknown point as shown in Figure 5d until the values of the variables are known at all nodes within the zone defined by the boundary CABD.

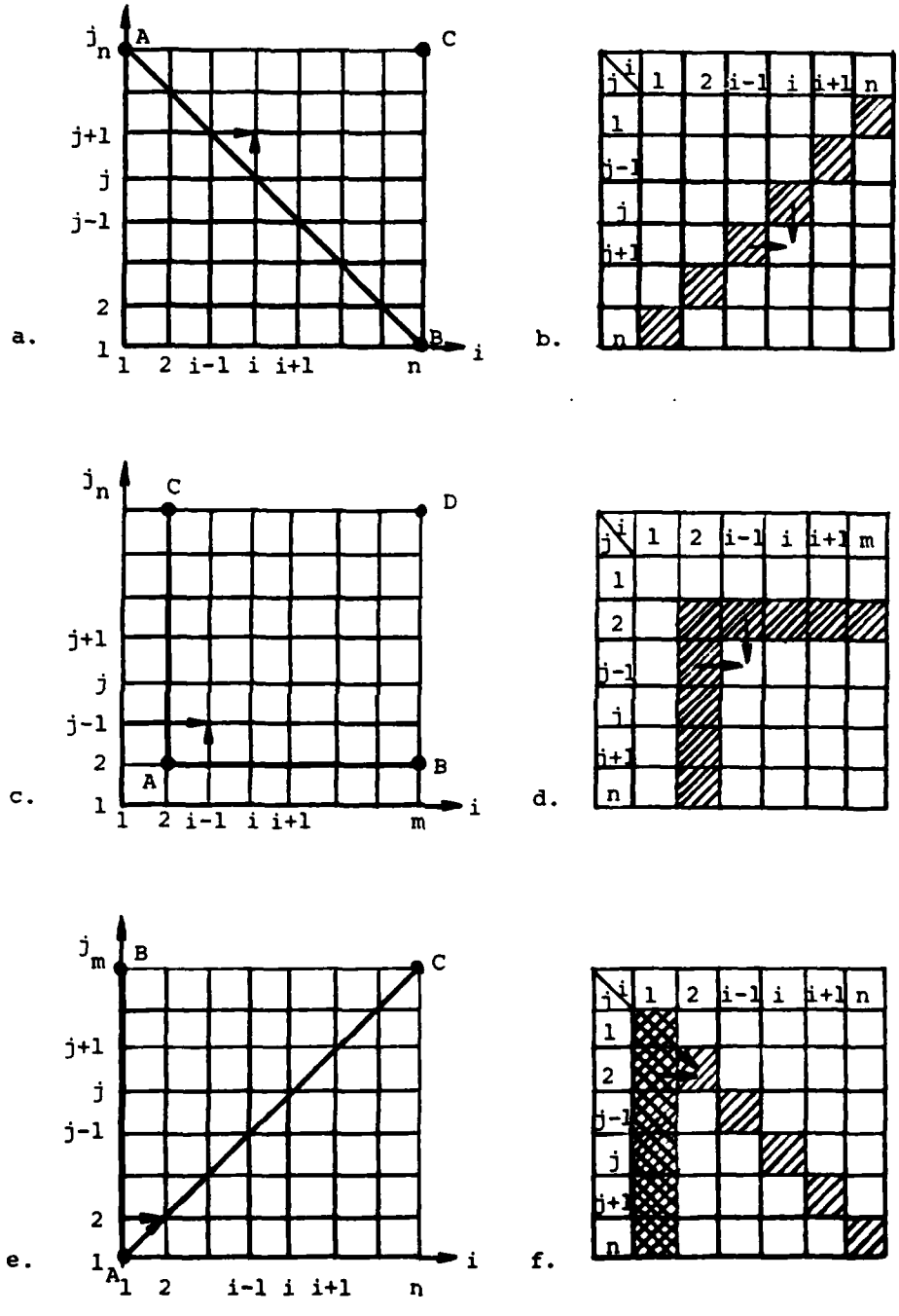

Figure 5. Type of boundary-value problems (after Harr, 1966). -- (a,b) Cauchy problem; (c,d) Goursat problem; (e,f) Mixed boundary-value problem.

Mixed Boundary-Value Problem

In this problem, some of the quantities x, z, σ, and θ are known and some specified along one (noncharacteristic) boundary and all of the quantities are known along another (characteristic) boundary. Thus there are a number of variations of this case. Figures 5e and 5f show one case where x, z, σ, and θ are all known along the characteristic AB and only z and σ are known along the non-characteristic line AC. The problem is to determine the value of all quantities on and within the boundary ABC. The recurrence formulas given by Equations 8 will not directly provide the results along AC. If Equations 7c and 7d are rewritten as:

$$x_{i,j} = (z_{i,j} - z_{i-1,j}) \cot (\theta_{i-1,j} - \mu) + x_{i-1,j} \tag{9a}$$

$$\theta_{i,j} = \theta_{i-1,j} + \frac{\{\gamma[(z_{i,j}-z_{i-1,j})-(x_{i,j}-x_{i-1,j})\tan\phi]+(\sigma_{i,j}-\sigma_{i-1,j})\}}{2\sigma_{i-1,j}\tan\phi} \tag{9b}$$

the resulting expression can be used to determine values along AC. For points within the boundary, where neither x, z, σ, or θ are known, Equations 8 must be used.

Once the desired x, z, σ, and θ quantities have been obtained, plotting and connecting the corresponding x and z coordinates of the same characteristics results in the slip line field. The envelope of these is the failure surface.

The corresponding stresses at any point can be obtained by extrapolating the σ and θ values at the nodal points and applying Equations 2. The accuracy of the results increases as the number of characteristics used in the grid increases. For increased accuracy, Sokolovskii recommended that, in Equations 8 and 9, the terms $\theta_{i-1,j}$ be replaced by $(\theta_{i-1,j} + \theta_{i,j})/2$ and $\theta_{i,j-1}$ by $(\theta_{i,j-1} + \theta_{i,j})/2$. Once $\theta_{i,j}$ is determined, $\theta_{i-1,j}$ and $\theta_{i,j-1}$ are recalculated, as just described, and substituted into the recurrence formulas, Equations 8 and 9.

Plasticity Approach to Retaining Wall Problem

The determination of lateral earth pressures against rigid retaining structures is one of the most common problems encountered in the evaluation of the stability of such structures. In practice, the Coulomb solution is widely used. This solution is a limit equilibrium solution in which the soil is assumed to fail by sliding along some plane inclined at a certain angle, ω, from the backface of the wall (refer to Figure 6). The magnitude of the angle ω is a function of the internal friction angle, ϕ, of the soil behind the wall, the wall-soil interface friction angle, δ, the wall backface inclination, α, with respect to the horizontal, and the backfill inclination, β, with respect to the horizontal. The magnitude of the force exerted by the backfill soil on the

wall depends upon the direction of wall movement. Wall movement away from the backfill is called the "active" case and wall movement into the backfill the "passive" case. Conditions imposed by anchor pullout approximate the passive case most closely. In the passive case (wall movement into the backfill) the soil-wall interface friction angle, δ, may be positive or negative. It is positive for downward movement of the wall relative to the backfill and negative for upward movement of the wall relative to the backfill. The (+) and (-) directions are shown in Figure 6. Therefore, the wall force, P_p, may act in any direction.

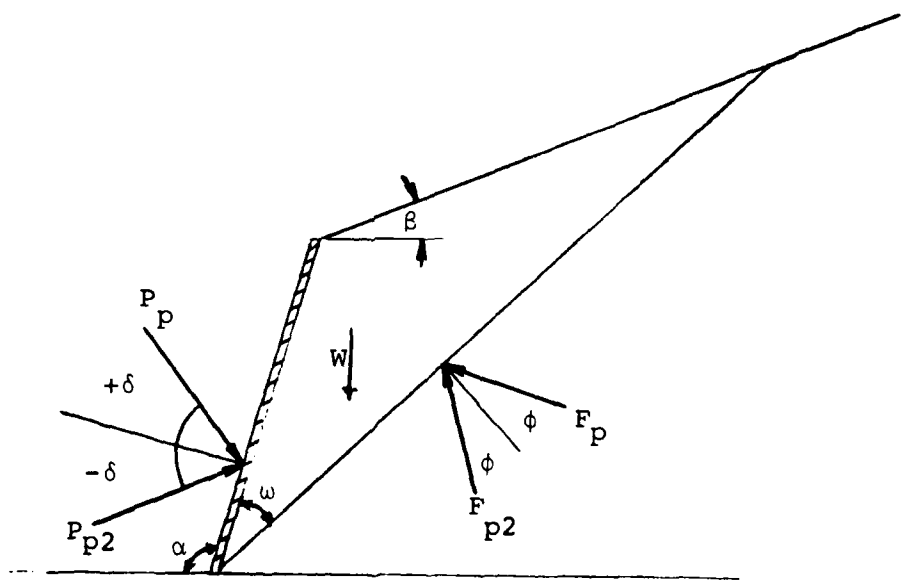

Figure 6. Coulomb solution to lateral earth pressure problems (after Nowatzki and Karafiath, 1981).

Positive δ angles are usually encountered in conventional soil mechanics problems where passive pressures are generated by horizontal movement of the wall into the soil backfill, i.e., the passive force of the wall against the backfill is directed downward. In some cases, however, such as soil anchors, bulldozer blades and track grousers, the force is applied at a negative δ angle.

Application of conventional plasticity theory to the problem of passive earth pressure results in slip line fields that define the geometry of the failure surface. The failure surfaces shown in Figures 7a and 7b compare well with those shown in literature, as, for example, by Chen (1975). The plasticity solution for the case shown in Figure 7c, however, results in an overlapping of the slip line field. This overlapping implies that two different stress states exist at a given point within the overlap region at the same time, a physical impossibility. Yet, plastic zones have been observed to form experimentally even for the case $\delta < 0$ (Rowe and Peaker, 1965).

In plasticity solutions obtained in the conventional way, all three boundary value problems are generally solved in order to obtain a complete slip line field within a loaded soil mass. Generally, the Cauchy problem is solved to obtain the passive zone, the Mixed Boundary-

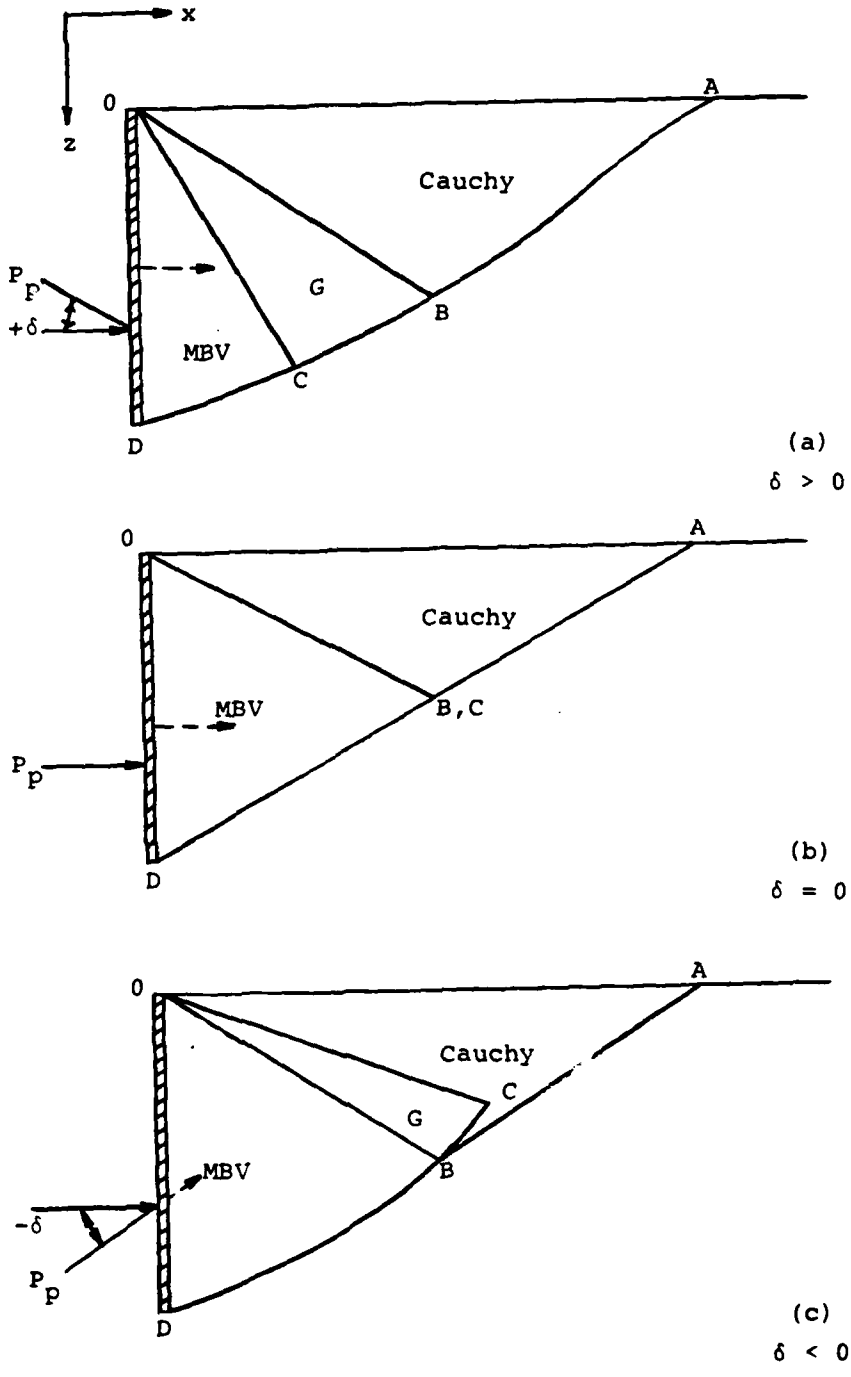

Figure 7. Passive case failure zone geometries for various values of δ (after Nowatzki and Karafiath, 1981).

Value problem (MBV) to obtain the active zone, and the Goursat problem (G) to obtain the transition zone between the other two.

These zones and their related problems are indicated in Figure 7 for the case of passive earth pressure on a retaining wall. Zone OAB is the Cauchy zone and zone OBC the Goursat zone. The computation of x, z, σ, and θ revolves about the singular point 0 where σ values are computed for specified changes in θ. In zone ODC, x, z, σ, and θ are known along OC after the Goursat problem has been solved. For a vertical wall, OD, x = 0 along the wall boundary and θ is assumed. Therefore, this is a Mixed Boundary-Value problem. Once solved, the normal pressures along the wall can be determined from σ and θ.

Reexamination of the boundary conditions by Nowatzki and Karafiath (1981) for this case resulted in the following conclusions:

1. In the passive case the wall force is an applied force, the direction of which is defined by the problem. Therefore, along OD (refer back to Figure 7) all four variables, x, z, σ, and θ, are given a priori (although for computational purposes σ and θ are assumed). Therefore, zone OBD should be solved as a Cauchy problem.

2. In cohesionless soils, θ along the free surface, OA, is undetermined since $\sigma_1 = \sigma_2 = \sigma_3 = 0$. Therefore, zone OAB should be solved as a Mixed Boundary-Value problem, with $z = 0$ and $\sigma = 0$ along OA.

Nowatzki and Karafiath developed a computer program incorporating the recurrence relationships of Equations 8 and 9, to accommodate the above boundary conditions. There was found to be excellent agreement between the computed and observed failure surfaces of cases investigated by Rowe and Peaker (1965). In addition, this new analytical approach does not contain the physically inadmissible overlapping of the slip lines previously encountered in application of plasticity theory to such problems, nor does it require an assumption of stress discontinuity within the slip line field as made by other researchers, as, for example Lee and Herrington (1972). The θ values vary along the ground surface, OA, indicating that the principal stresses reorient themselves as a result of the upward pushing of the wall. In this procedure, zone OCB disappears, since there is no stress discontinuity at 0 in this direction.

CHAPTER 3

LITERATURE REVIEW OF ANCHOR PULLOUT STUDIES

Baker and Konder (1966) summarized the failure hypotheses for shallow anchors by the "friction cylinder method," the "soil cone method" and Balla's method. The shapes of the corresponding failure surfaces are shown in Figure 8. In the friction cylinder method, the pullout capacity, P, is equal to the weight of soil, W_s, immediately above the anchor as well as the shear resistance, S, along the assumed vertical cylindrical failure surface. The soil cone method assumes that the failure surface takes the shape of a truncated cone extending above the anchor with a base angle of $45^{\circ} - \phi/2$. The pullout capacity is given as the weight of the soil within the truncated cone. The method presented by Balla (1961) is based on the shape of the failure surface observed during small-scale model anchor tests (Figure 8c) in sand. The pullout capacity is equal to the weight of soil within the assumed failure surface and the side shear resistance.

Prediction of the pullout capacity of a buried circular plate is accomplished by the following equation:

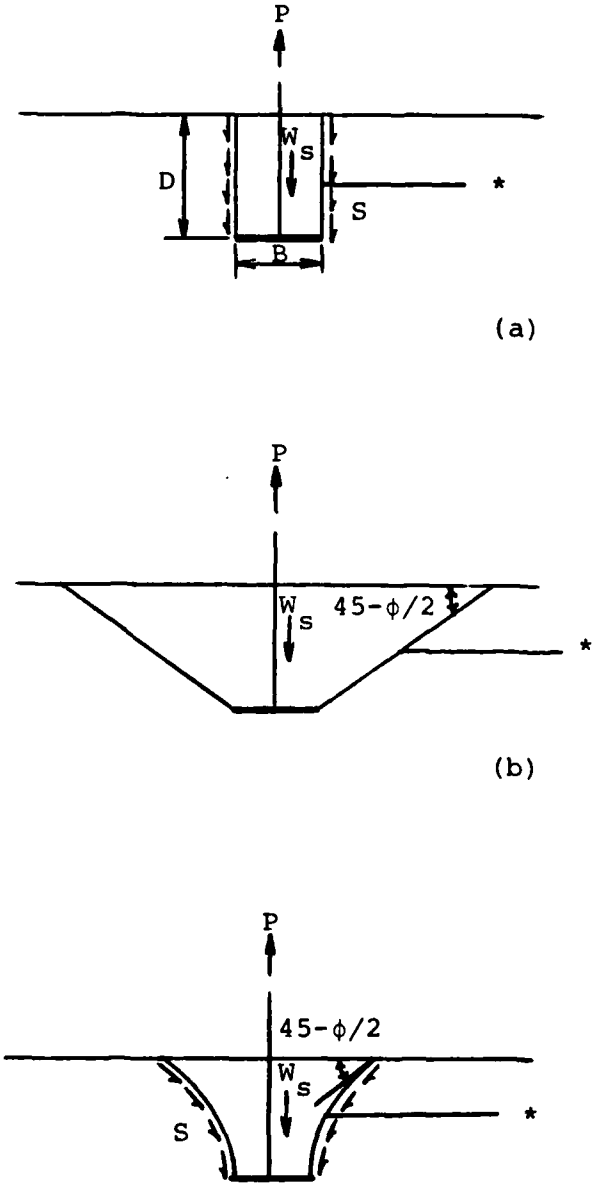

Figure 8. Methods of calculating pullout capacity (after Baker and Konder, 1966). -- (a) Friction cylinder method; (b) Soil cone method; (c) Balla's method.

$$P = \gamma D F_q A \qquad (10)$$

where

A = projected area of the plate

D = depth of the anchor plate below the ground surface

F_q = a pullout factor which is a function of the angle of shearing resistance of the sand, and the D/B ratio

P = pullout capacity

γ = effective unit weight

Modern research on this subject began with the paper by Balla. Baker and Konder (1966) confirmed Balla's major findings regarding anchor plates in dense sand; they showed that deep anchors behaved differently from shallow anchors. Sutherland (1965) presented results of pullout tests with model plates up to 6 in. in diameter in loose and dense sand, as well as with 94 in. diameter shafts in medium dense to dense sands. He found that the mode of failure varied also with sand density and showed that Balla's analytical approach gave reasonable results only in sands of some intermediate density.

Vesic (1971) showed that his theory of expansion of cavities close to the surface of a semi-infinite rigid-plastic solid, which gives the ultimate radial pressure needed to

break out a cylinder or a spherical cavity, can be applied to the problem of anchor plates. Vesic found that transition to deep anchor behavior occurred in loose sand at D/B ratios of two or three, and in dense sand at D/B ratios of ten or more.

Healy (1971) performed both model and field pullout tests in granular materials. He found that the pullout resistance of small anchors (6 inches) in sand varied directly with the depth provided that the anchors have D/B ratios equal to or greater than six in dense sand and D/B ratios between two and six in loose sands.

Adams and Hayes (1967) photographed pullout tests in sand for D/B ratios between 2 and 4.5. The failure surface changes with relative density and D/B ratio. At shallow depths ($D/B \simeq 2$), the failure shape very closely approximates the friction cylinder method assumption, regardless of the soil density. At greater depths ($D/B > 4.5$), the failure zone was "local" for a loose sand condition, while for the dense sand tests, the failure zone reached the ground surface.

Kovacs and Yokel (1979) summarized the studies of Bemben, Kupferman and Kalajian (1971), in which the pullout capacity of a 55 in^2 Y fluke (marine) anchor for various depths of embedment was presented as calculated by seven

different theoretical methods and as measured in field loading tests. There is some agreement between predicted and measured values for D/B ratios less than 3. At D/B = 4, the predicted pullout capacity varies considerably. As the anchor is embedded further, only the friction cylinder hypothesis gives reasonably conservative results. This was also observed by Das and Seeley (1975). Based on the wide scatter of the pullout factor, Fq versus D/B relationship as determined theoretically and in the laboratory, Esquivel-Diaz (1967) concluded that no satisfactory theory is available for the determination of the pullout capacity of circular disc anchors.

The anchor pullout studies discussed in this chapter apply only to dry sand. However, there are anchor pullout studies on clays and marine soils. An extensive bibliography of anchor pullout studies is contained in Kovacs and Yokel (1979).

CHAPTER 4

SOLUTION PROCEDURE

Definition of the Problem

Figure 9 shows the coordinate axis used in the problem. A circular disk is embedded at some depth, +z downward, below the surface. A force, P, acting along the z-axis in the negative direction, is applied at the center of the plate. The problem is axially symmetric with respect to geometry and load. Therefore, only half the problem needs to be solved. Assumptions inherent to this study are:

1. Soil behaves as a rigid-perfectly plastic material.
2. Soil strength properties are homogeneous and isotropic.
3. Seepage and inertia forces are equal to zero.
4. There are no normal or shear stresses along the ground surface.
5. The anchor plate is infinitely rigid with respect to the soil, so that the soil fails before the anchor plate deforms.

The primary difficulty is determining the boundary conditions. It was hypothesized that as the plate is moved

upward, a mass of soil above the plate moves with it as a rigid body. The movement of this rigid body of soil stresses the surrounding soil, and thereby creates the slip line field at failure. The shape of the rigid body is not known. Two shapes were arbitrarily selected and investigated separately in this study. The first was a right circular cone, with the apex at the surface and the base coincident with the plate (Figure 9a). The second was a right circular cylinder extending vertically from the edge of the plate to the surface (Figure 9b) and having the same diameter as the plate itself.

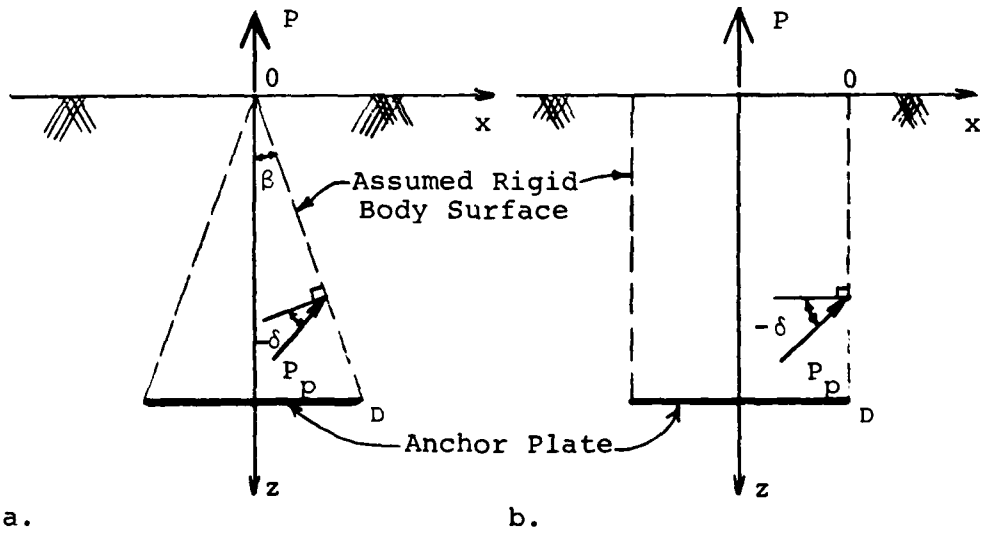

Figure 9. Assumed rigid body surfaces.

The stresses transferred from the rigid body to the surrounding soil are due to passive pressures, with $\delta < 0$ generated at the soil-rigid body interface. Therefore, the analytical

approach of Nowatzki and Karafiath (1981) was extended to the problem at hand, with the rigid body surface acting similar to a retaining wall boundary.

Procedure

Nowatzki and Karafiath's computer program was altered, and the boundary conditions outlined in the previous section were incorporated. The program for each rigid body is included in Appendix A. Figure 10 shows the numbering of nodal points and the layout of the problem for computer solution. The solution procedure is demonstrated schematically in Figure 11. Equations 9 were used to determine x and θ values along the ground surface, OA, and Equations 8 were used to compute x, z, σ, and θ values of the remaining nodal points. Figure 10 also shows the plot of θ values along the ground surface, with negative θ values shown upward.

Although $z = 0$ and $\sigma = 0$ along the ground surface, OA, an explanation is required of how the parameters were obtained along the rigid body surface, OD. After the soil parameters and the geometry of the problem are input, the program divides the boundary OD into $(n - 1)$ equal segments (refer to Figure 10), where n = some convenient number of nodal points. For the cylindrical rigid body surface, $x = 0$ and Δz = depth of the plate/$(n - 1)$. For the cone surface, Δx = plate radius/$(n - 1)$ and Δz = depth/$(n-1)$.

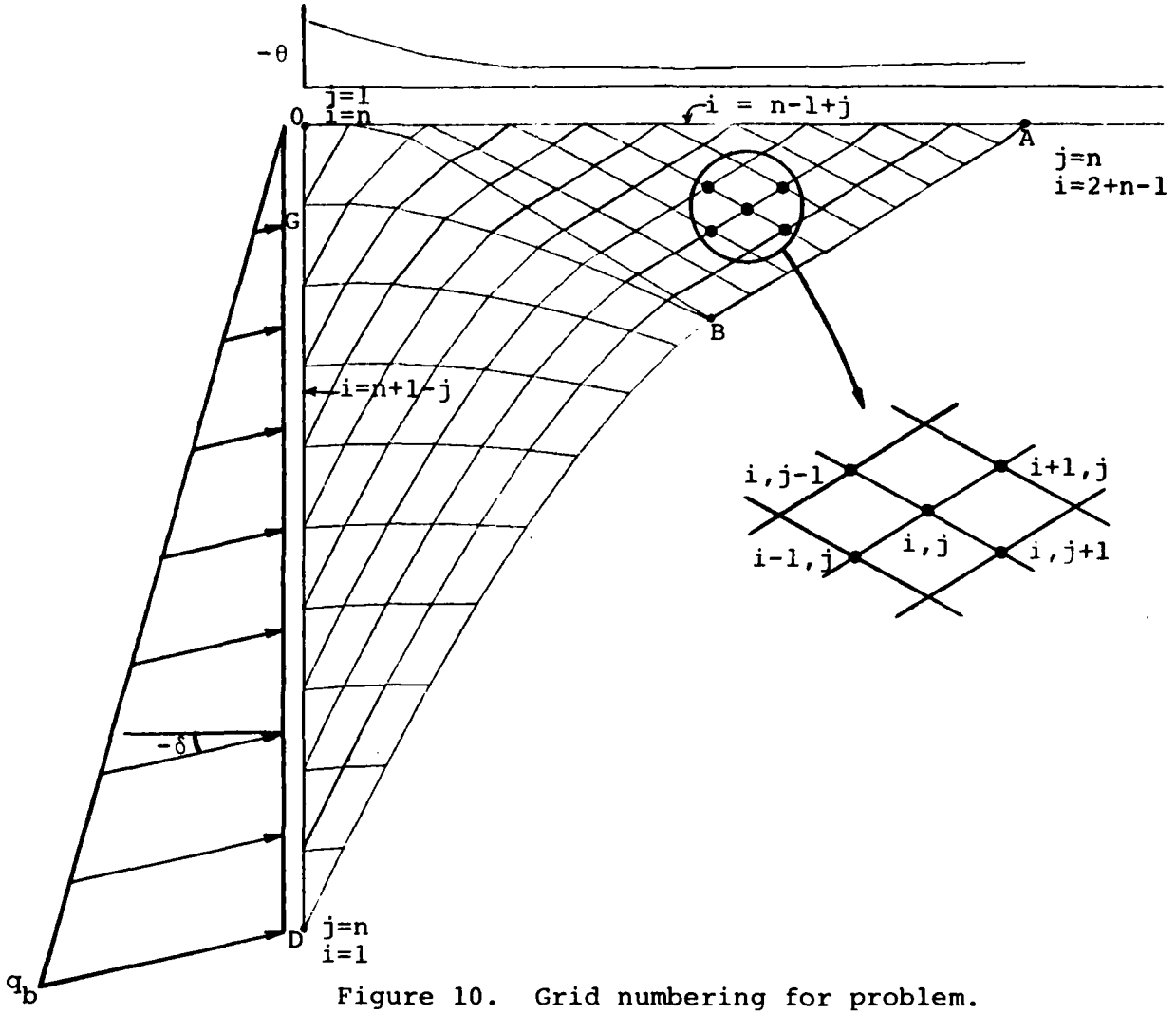

Figure 10. Grid numbering for problem.

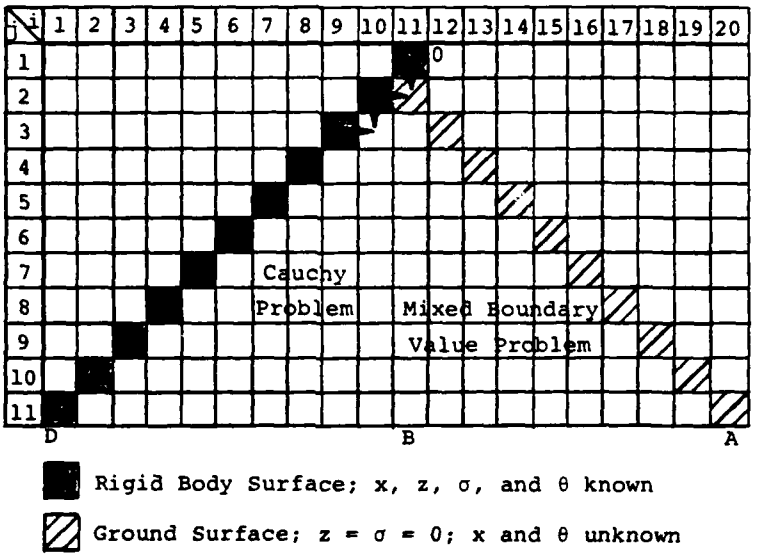

Figure 11. Solution procedure.

Along both surfaces, δ was assumed to remain constant and the surface load varied linearly from zero at the surface, point 0, to the maximum value at the base, point D. The stress at this point was designated q_b. The magnitude of δ and q_b was estimated and input for an initial trial. Then, θ and σ at point D was determined using the following relationships:

$$\theta = (1/2)\arctan \frac{\sin\left(\frac{\sin\delta}{\sin\phi}\right)}{\sqrt{1-\left(\frac{\sin\delta}{\sin\phi}\right)^2}} + (\delta/2) \qquad (11a)$$

$$\sigma = \frac{q_b}{\cos\delta + \sqrt{\cos^2\delta - \cos^2\phi}} \qquad (11b)$$

For the rigid body cone, the inclination of the rigid body surface (i.e., angle β of Figure 9a) had to be taken into account in determining θ.

The above procedure required assuming various combinations of δ and q_b values, because many of these assumed combinations of values did not create a proper slip line field (i.e., overlaps occurred within the slip line field). A solution was assumed to be acceptable when, for a given q_b, δ was varied until ocerlapping in the slip line field was eliminated. The acceptable combination of δ and q_b that predicted the greatest pullout capacity was assumed to be the correct one.

Figures 12 through 15 demonstrate the variations in the slip line field with different assumed δ and q_b along the rigid body surfaces. These figures also show the variations in θ along the ground surface. In each of these figures the middle plot was assumed to be the correct slip line field. To produce Figures 12 and 13, δ value remained constant and the surface loading was progressively increased from (a) to (c). Overlaps within the slip line field are circled. For Figures 14 and 15, the surface loading remained constant and δ values were varied, becoming increasingly more negative from (a) to (c). Note that Figures 14a and 15a are also acceptable slip line fields. However, neither is considered to be the correct one, in accordance with assumptions stated in previous paragraphs.

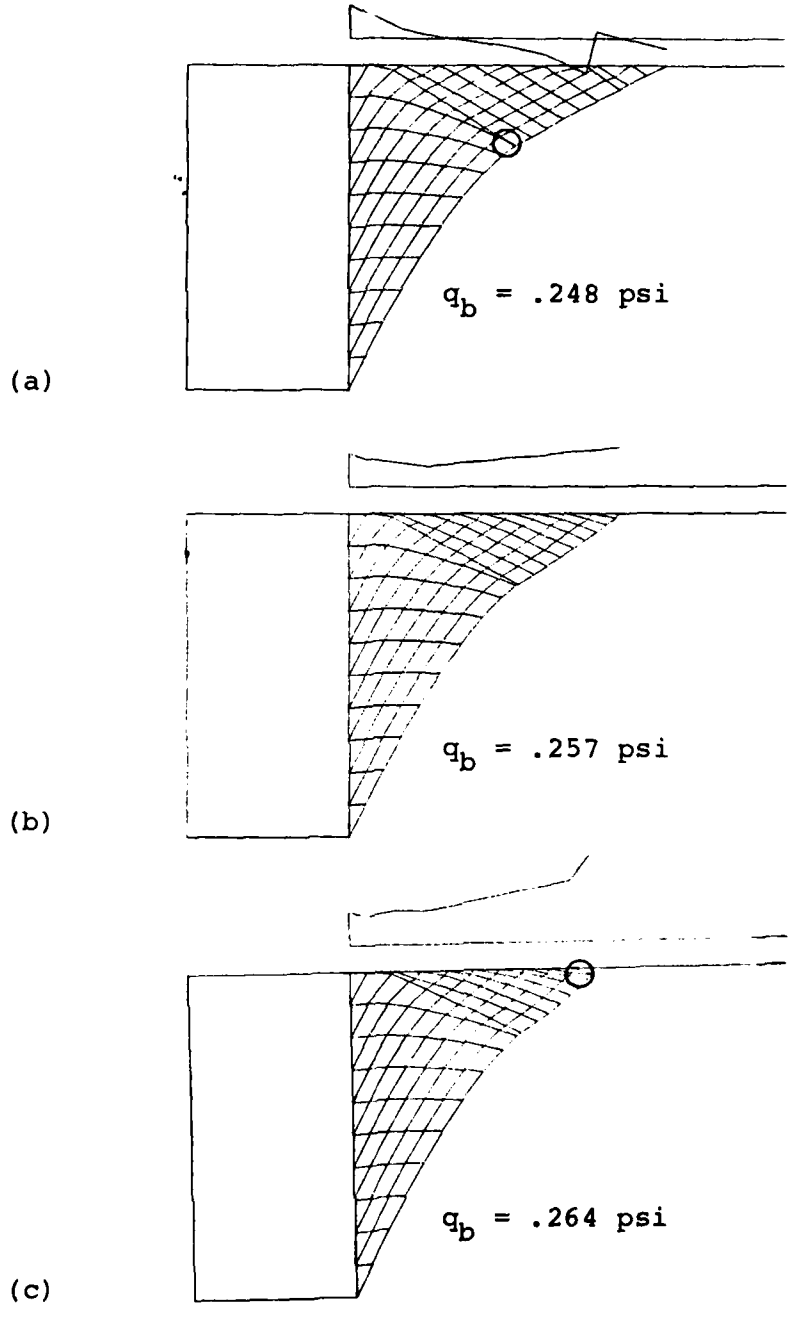

Figure 12. Variation of surface load (cylinder). -- $\delta = -23.0^{\circ}$, B = 3", D = 3".

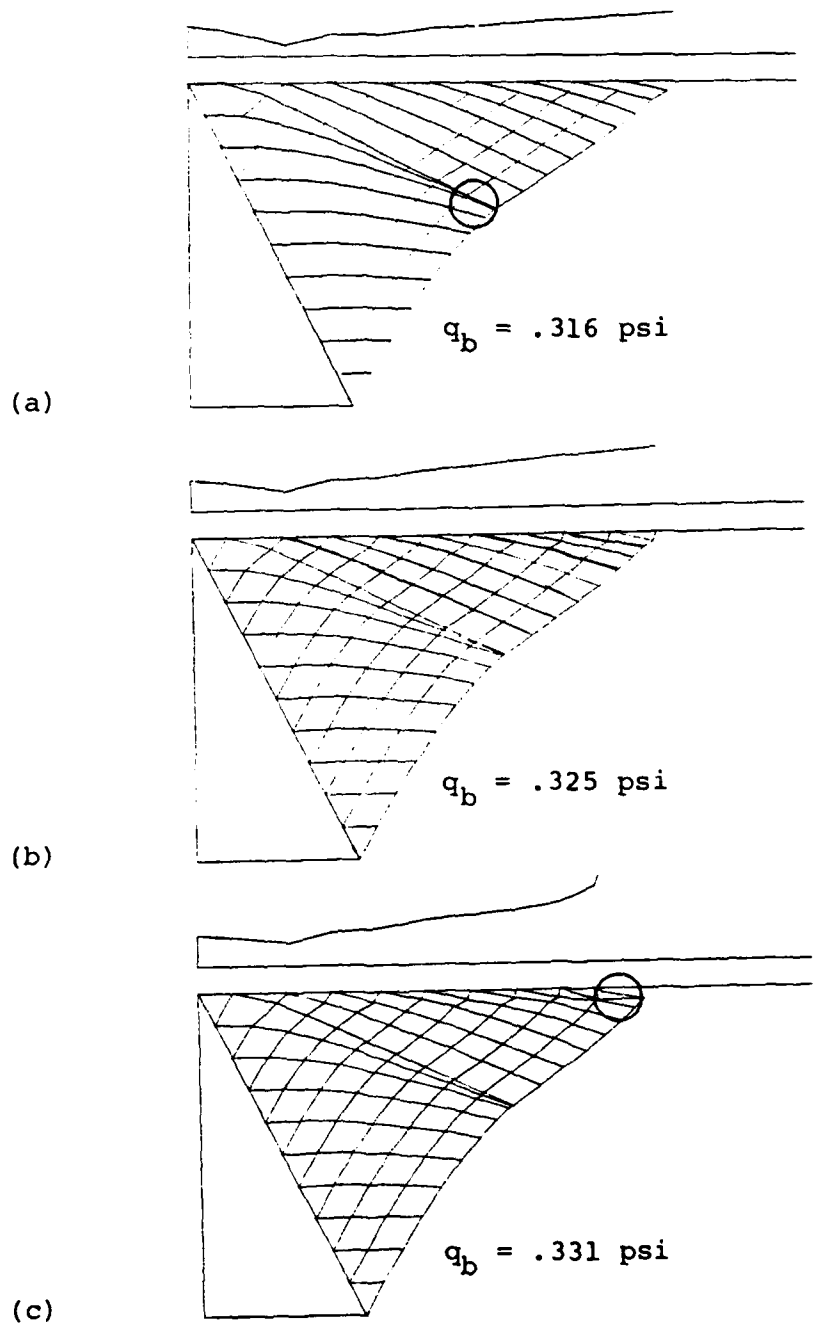

Figure 13. Variation of surface load (cone). -- $\delta = -4.0^{o}$, B = 3', D = 3".

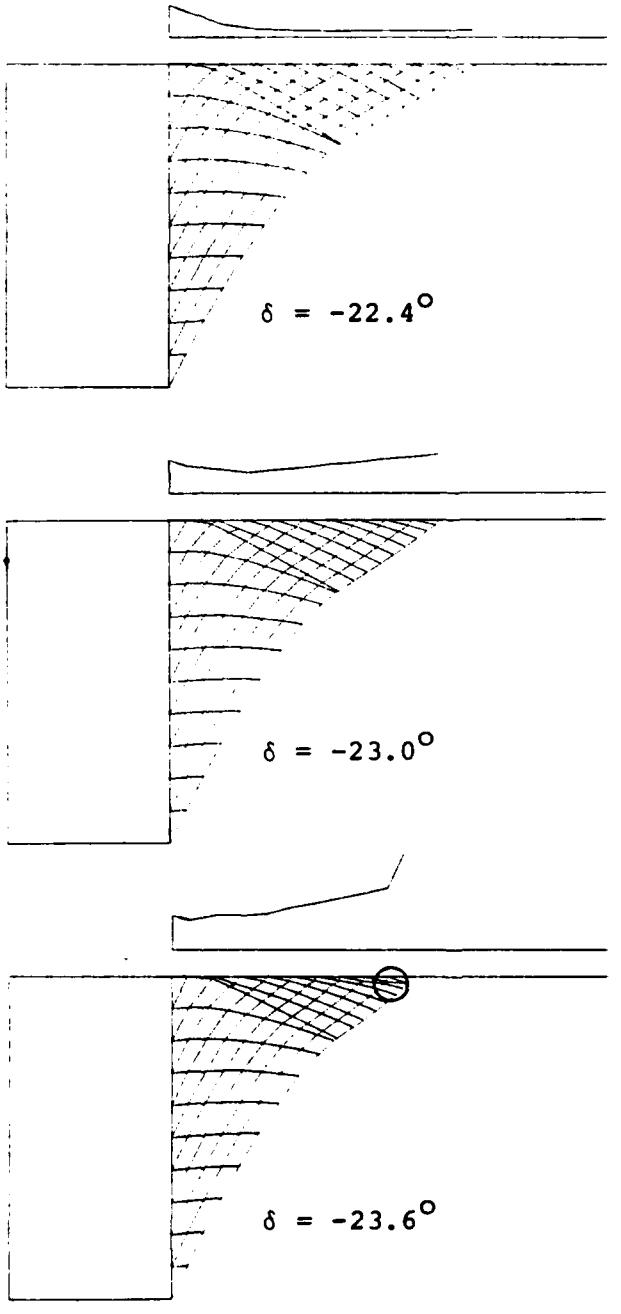

Figure 14. Variation of δ (cylinder). -- q_b = .257 psi, B = 3", D = 3".

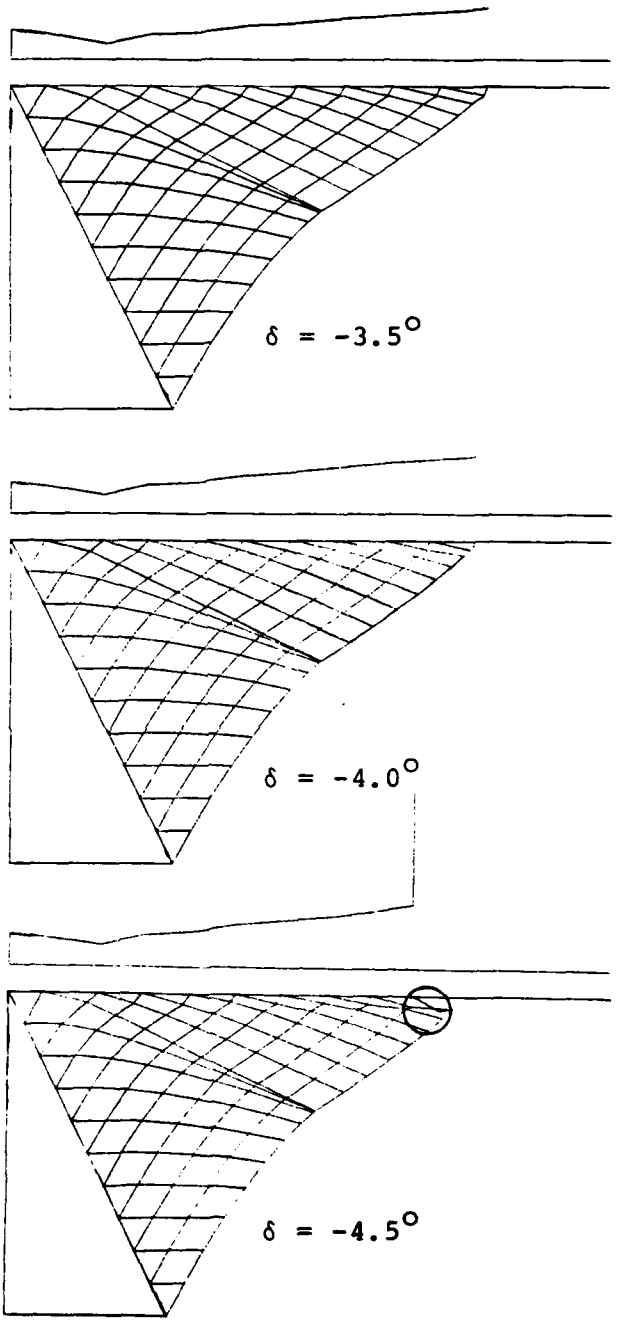

Figure 15. Variation of δ (cone). -- q_b = .325 psi, B = 3", D = 3".

The process of assuming various combinations of δ and q_b and evaluating the results with regard to permissible solutions was greatly facilitated by using the facilities of the University of Arizona Interactive Graphics Engineering Laboratory. Here the x, z, σ, and θ values for the j = n nodal points were viewed on the screen as they were calculated, i.e., in real time. Generally, if there was an overlap within the slip line field, it occurred on the j = n characteristic line. Plotting was then done as a check on what otherwise seemed an acceptable slip line field. Therefore, this iterative procedure was easily accomplished internal to the execution of the program. This procedure saved time, eliminated redundant calculations, and decreased the possibility for human error.

The CALPLOT program was used to plot the mesh of x and z values calculated and the θ values along the ground surface. The CALPLOT program consists of FORTRAN callable subroutines, each of which works through the computer hardware system to drive the Calcomp 602 plotter. A sample printout of slip line field values is included in Appendix B.

Once the correct slip line field was determined, the pullout capacity, P, and pullout factor, F_q, were calculated as follows. The z-direction component of q_b was designated as σ_z. Integration of the triangular stress distribution over the rigid body surface yielded the following expressions:

For the cone:

$$S = (1/2)\ \sigma_z\ \pi\ R\sqrt{R^2 + D^2} \qquad (12a)$$

For the cylinder:

$$S = \sigma_z\ \pi R\ D \qquad (12b)$$

Adding the shear resistance, S, to the weight of the soil within the rigid body yielded the pullout capacity as follows:

For the cone:

$$P = S + (1/3)\gamma\pi R^2 D \qquad (12c)$$

For the cylinder:

$$P = S + \gamma\pi R^2 D \qquad (12d)$$

Rewriting Equation 10 yielded the following expression for pullout factor:

$$F_q = \frac{P}{\gamma\pi R^2 D} \qquad (12e)$$

where

R = plate radius (B/2)

D = plate depth

γ = soil unit weight

The pullout factor is used in many studies to compare pullout capacity results with other reports. In this way, different sized anchors can be equated if their relative depth (D/B) and the soil parameters are the same.

CHAPTER 5

PRESENTATION AND DISCUSSION OF RESULTS

A summary of the numerical results for this study is given in Table 1. The relationship between pullout factor (F_q) and relative depth (D/B) determined in this study are plotted, along with other theoretical and experimental results in Figures 16a and 16b for loose and dense sand, respectively. In this study, loose sand was considered to have a unit weight of 100 pcf and an angle of internal friction of 31^o; dense sand was assumed to have γ = 112 pcf and $\phi = 42^o$.

The theoretical results of this study are lower than experimental findings, but are much closer at shallow depths, with the differences becoming progressively greater with depth. The rigid body cylinder assumption predicts higher pullout capacities than the cone. A numerical comparison of the theoretical F_q values with experimental ones is shown in Table 2. For D/B ratios down to four, the cylinder F_q values in loose sand are an average of 81 percent of Sutherland's results. At D/B = 1, theoretical values are in agreement with Vesic's Theory, but rapidly diverge with depth. For dense sand, the cylinder F_q values are an average

Table 1. Theoretical study results.

Rigid Body	D/B Ratio	Angle of Internal Friction (ϕ)	Unit Weight (pcf)	Pullout Capacity* (lb)	F_q
Cone	1	31	100	1.72	1.39
"	2	"	"	4.86	1.98
"	3	"	"	9.56	2.59
"	4	"	"	15.57	3.17
"	10	"	"		
Cylinder	1	"	"	2.63	2.14
"	2	"	"	8.07	3.29
"	3	"	"	16.33	4.44
"	4	"	"	27.36	5.57
"	10	"	"	152.94	12.46
Cone	1	42	112	2.35	1.70
"	2	"	"	7.05	2.56
"	3	"	"	14.13	3.43
"	4	"	"	23.57	4.28
"	10	"	"	129.33	9.41
Cylinder	1	"	"	3.73	2.72
"	2	"	"	12.19	4.44
"	3	"	"	25.36	6.14
"	4	"	"	43.28	7.87
"	10	"	"	249.84	18.18

* For 3" diameter plate.

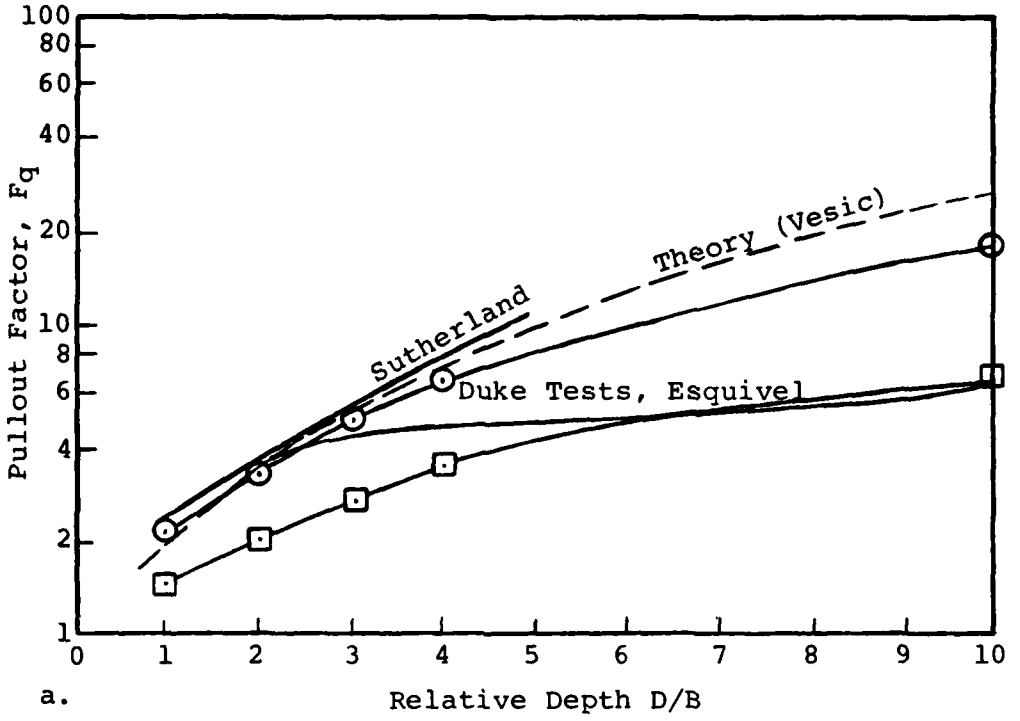

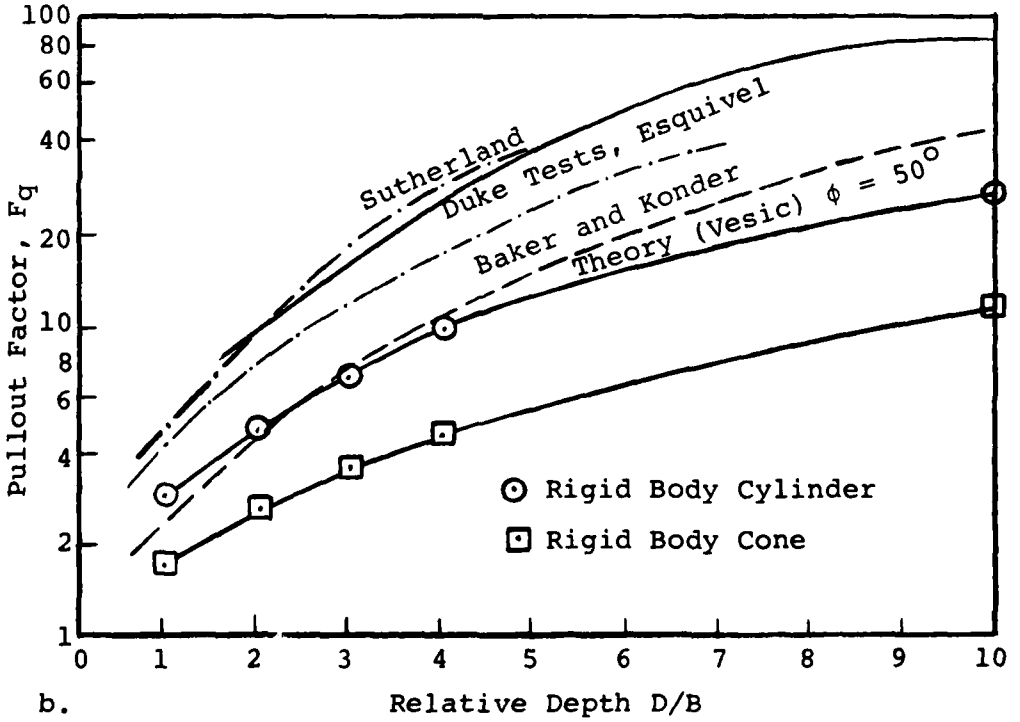

Figure 16. Comparison with other studies. -- (a) Loose sand; (b) Dense sand.

Table 2. Numerical comparison of F_q values.

		Rigid Body			
	D/B	Cylinder	Cone	Sutherland	Vesic
Loose Sand					
	1	2.1	1.4	2.5	2.1
	2	3.3	2.0	3.8	3.5
	3	4.4	2.6	5.4	5.4
	4	5.6	3.2	7.7	7.6

		Rigid Body			
	D/B	Cylinder	Cone	Sutherland	Baker & Konder
Dense Sand					
	1	2.7	1.7	4.8	4.0
	2	4.4	2.6	10.1	6.5
	3	6.1	3.4	19.3	12.0
	4	7.9	4.3	29.8	17.3

of 58 percent of Baker and Konder's and 40 percent of Sutherland's results.

Figure 17 shows that theoretical pullout factors increase linearly with relative depth increase. In contrast, experimental F_q values appear to increase exponentially with increasing relative depth.

The causes of the disagreement with observed data were not determined. However, the assumption of linearly varying σ and/or constant θ/δ along the surface of the rigid body, could be refined. Varying these parameters along the rigid body surface might produce an acceptable slip line field at a more inclined δ, thus mobilizing more shear strength of the soil and increasing the predicted pullout capacity. Perhaps another rigid body shape is correct, possibly a cone truncated at the ground surface, or an elliptical or parabolic rigid body surface. Investigation of these shapes was beyond the scope of this study.

It should be noted that the plane strain equations were used in this analysis, and not the axially symmetric ones. The latter equations are presented in Karafiath and Nowatzki (1978).

Attempts were made to use the recurrence relationships for the axially symmetric case; however the solutions did not converge. It is felt that the boundary conditions imposed by the anchor pullout problem made the recurrence relationships ill-conditioned for the numerical method followed in the plane strain solution procedure.

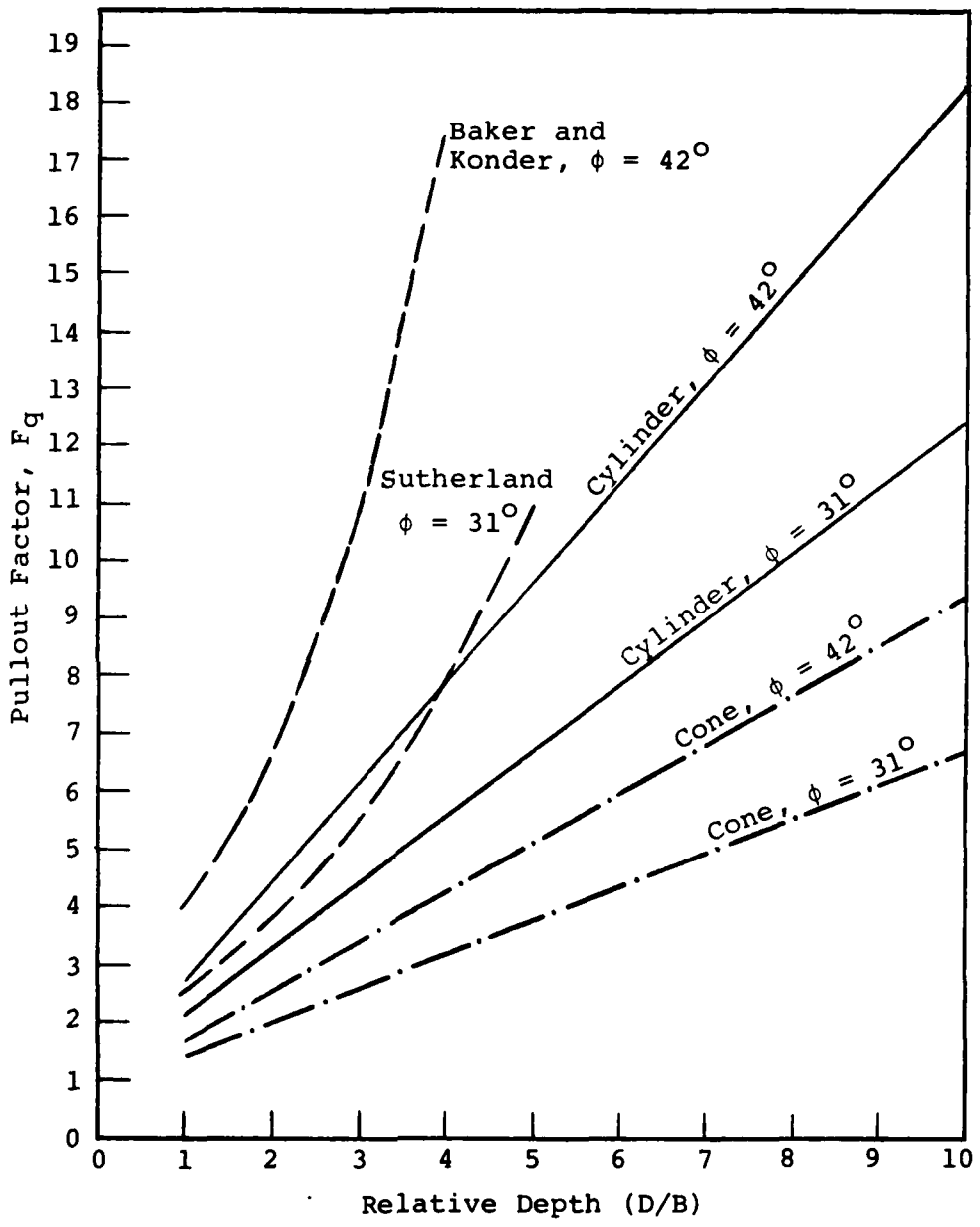

Figure 17. Comparison with selected studies.

Comparison with Coulomb Trial Wedge Method

Since not all engineers have ready access to a computer, it was desired to find an easy hand method to approximate the theoretical analysis. It was found that the results of the Coulomb graphical trial wedge method (see Figure 18) correlated well with the computer results. For $\delta = 0.75\theta$ as obtained from the computer solution, the most critical failure wedge with the rigid body surface was found to be approximately 30^{o} for both the loose and dense soil. The Z-directional component of the measured P_p force was integrated over the circumference of the rigid body cylinder and then added to the weight of the soil within the rigid body cylinder to determine the pullout capacity, P. The pullout factor, F_q, was then calculated using Equation 12e. There is a very close correlation between the results of the computer analysis and those of the trial wedge method. The comparison is shown in Table 3.

Thus it seems that the graphical solution could be used just as well as the sophisticated computer solution to obtain an estimate of Pullout Factor F_q for the conditions and assumptions made in this study. Obviously, both solutions fall short of the test data, indicating that the plane strain assumption may be unrealistic for this case.

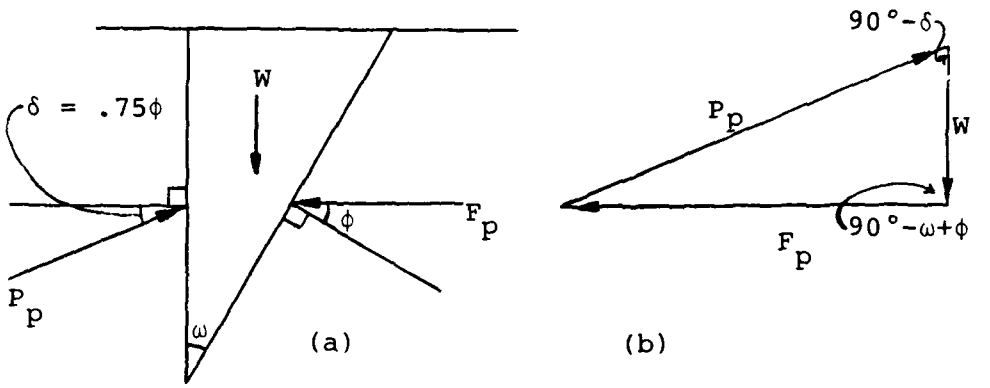

Figure 18. Trial wedge method. -- (a) Failure wedge and acting forces; (b) force polygon for computation of P_p.

Table 3. Correlation between computer analysis and trial wedge method F_q values.

D/B	ϕ	Computer	Trial Wedge
1	31°	2.14	2.17
2	31°	3.29	3.33
3	31°	4.44	4.50
4	31°	5.57	5.67
1	42°	2.72	2.75
2	42°	4.44	4.50
3	42°	6.14	6.24
4	42°	7.87	7.99

CHAPTER 6

CONCLUSIONS

This has been a theoretical anchor pullout study, using the plasticity theory and hypothesis that a rigid body of soil moves with the anchor plate as it is moved toward the surface. Two such rigid body shapes were investigated: the right circular cylinder and right circular cone. The theoretical pullout capacities were found to be lower than experimental results, with the cylinder rigid body providing closer agreements than the cone. At shallow depths in loose sand, predicted pullout capacities are approximately 81 percent of experimentally determined ones. In dense sand, predicted values are about 50 percent of experimental ones.

Assumptions of this report might be changed to provide better results. Varying δ and/or applying a non-triangular stress distribution along the surface may produce acceptable slip line fields at a more inclined δ, thus predicting a greater pullout capacity. Additionally, there is also the possibility that neither of the rigid body surfaces investigated are the correct ones.

A conventional, graphical solution procedure was also used to determine the pullout capacity. The results of that solution correlate well with the computer results. This suggests that small engineering offices, without access to a computer, may be able to utilize simpler, approximate solutions for anchor pullout problems provided the conditions assumed in this study pertain.

Recommendations for Further Study

1. Refine the mathematical model to account for variable δ and/or variable stress distribution along the rigid body surface.
2. Investigate other possible rigid body surfaces, such as a truncated cone, ellipse, or parabola.
3. Perform full-scale and model tests.
4. Further study of the axially symmetric computer solution.

APPENDIX A

COMPUTER PROGRAMS

```
C                    CONE RIGID BODY
      DIMENSION X(21,11),Z(21,11),SIG(21,11),THE(21,11)
      OPEN 12,"ARRAYS.OUT",ATT="SOM"
      ACCEPT "INPUT PHI,GAMMA=  ",PHI,GAMMA
      TYPE "   PHI=",PHI,"   GAMMA=",GAMMA
      ACCEPT "INPUT DEPTH,LENGTH ",DEPTH,HLENG
      TYPE "DEPTH=",DEPTH,"   LENGTH=",HLENG
      ACCEPT "INPUT N ",N
      TYPE "N=",N
      GO=GAMMA
      ARC=.0174533
      PI=3.14159
      F1=ARC*PHI
      TF=TAN(F1)
      U1=PI/4-F1/2
   59 DO 58 J=1,N
      DO 58 I=1,21
      X(I,J)=0
      Z(I,J)=0
      SIG(I,J)=0
   58 THE(I,J)=0
      NT=N
      ACCEPT "INPUT DELTA,QBOT ",DELTA,QBOT
      TYPE "DELTA=",DELTA,"  QBOT=",QBOT
      DEL=ARC*DELTA
      BETA=ATAN(HLENG/DEPTH)
      DTHE=.5*(ATAN(SIN(SIN(DEL)/SIN(F1))/
    1 SQRT(1-(SIN(DEL)/SIN(F1))**2))+DEL)-BETA
      SIBOT=QBOT/(COS(DEL)+SQRT(COS(DEL)**2-COS(F1)**2))
      DO 80 J=1,N
      I=N+1-J
      F=(FLOAT(J)-1)/(N-1)
      X(I,J)=F*HLENG
      Z(I,J)=F*DEPTH
      SIG(I,J)=F*SIBOT
   80 THE(I,J)=DTHE
      IF(ABS(THE(N,1)).GT.U1) NT=N-1
      TYPE "THE,U1=",THE(N,1),U1
      DO 90 J=2,N
      DO 90 I=(N+2-J),(NT+J-1)
      IF(I.EQ.(NT+J-1)) GO TO 10
      L=0
      TH1=THE(I,J-1)+U1
      TH2=THE(I-1,J)-U1
      SI1=SIG(I,J-1)
      SI2=SIG(I-1,J)
      V7=2*SIG(I-1,J)*SIG(I,J-1)
      U9=SIG(I-1,J)+SIG(I,J-1)
      V8=(THE(I,J-1)-THE(I-1,J))*TF
      V9=2*SIG(I-1,J)*SIG(I,J-1)*V8
      U6=2*TF*(SIG(I,J-1)*THE(I,J-1)+SIG(I-1,J)*THE(I-1,J))
    5 V1=TAN(TH1)
      V2=TAN(TH2)
      XI=V1*X(I,J-1)
      XJ=V2*X(I-1,J)
      V12=1/(V1-V2)
      X(I,J)=V12*(Z(I-1,J)-Z(I,J-1)+XI-XJ)
      Z(I,J)=Z(I-1,J)+(X(I,J)-X(I-1,J))*V2
      AA=-TF*(X(I,J)-X(I-1,J))+(Z(I,J)-Z(I-1,J))
      BB=TF*(X(I,J)-X(I,J-1))+(Z(I,J)-Z(I,J-1))
      U5=SIG(I,J-1)-SIG(I-1,J)
      IF(U9.EQ.0) GO TO 15
      SIG(I,J)=(V7+V9+GO*(SI1*AA+SI2*BB))/U9
      THE(I,J)=(U5+U6+GO*(BB-AA))/(2*TF*U9)
```

```
      GO TO 16
15    SIG(I,J)=GO*(AA+BB)/(2+TF*(THE(I-1,J)-THE(I,J-1)))
      THE(I,J)=(BB*(1+THE(I-1,J))-AA*(1-THE(I,J-1)))/(AA+BB)
16    IF(L.EQ.1) GO TO 20
      TH1=.5*(THE(I,J-1)+THE(I,J))+U1
      TH2=.5*(THE(I-1,J)+THE(I,J))-U1
      SI1=.5*(SIG(I,J-1)+SIG(I,J))
      SI2=.5*(SIG(I-1,J)+SIG(I,J))
      U6=2*TF*(SI1*THE(I,J-1)+SI2*THE(I-1,J))
      V7=SI1*SIG(I-1,J)+SI2*SIG(I,J-1)
      V9=2*SI1*SI2*V8
      U9=SI1+SI2
      L=1
      GO TO 5
10    Z(I,J)=0
      SIG(I,J)=0
      TH3=TAN(THE(I-1,J)-U1)
      KK=0
11    X(I,J)=X(I-1,J)-Z(I-1,J)/TH3
      AA=-TF*(X(I,J)-X(I-1,J))+(Z(I,J)-Z(I-1,J))
      U3=SIG(I,J)-SIG(I-1,J)-GO*AA
      THE(I,J)=U3/(2*SIG(I-1,J)*TF)+THE(I-1,J)
      TH3=TAN(.5*(THE(I,J)+THE(I-1,J))-U1)
      IF(KK.EQ.6) GO TO 20
      KK=KK+1
      GO TO 11
20    IF(J.EQ.N) TYPE "I,J,X,Z= ",I,J,X(I,J),Z(I,J)
90    CONTINUE
      SIZ=QBOT*SIN(BETA-DEL)
      S=.5*SIZ*PI*HLENG*SQRT(HLENG**2+DEPTH**2)
      P=S+GO*PI*HLENG**2*DEPTH/3
      FQ=P/(GO*DEPTH*PI*HLENG**2)
      TYPE "P=",P,"  FQ=",FQ
      ACCEPT "INPUT 1 FOR CHANGE OF DATA,ELSE 0 ",IJK
      IF(IJK.EQ.1) GO TO 59
      ACCEPT "INPUT 1 FOR PRINT OF DATA,ELSE 0 ",KJI
      IF(KJI.EQ.0) GO TO 75
      WRITE (12,24)
24    FORMAT (/39X,"CONE RIGID BODY"/"PHI,GO,DEPTH,HLENG,QBOT,",
     1 "P,FQ,DELTA")
      WRITE (12,25) PHI,GO,DEPTH,HLENG,QBOT,P,FQ,DELTA
25    FORMAT (10F10.4)
      WRITE (12,30)
30    FORMAT (//40X,"X-COORDINATES"//)
      WRITE (12,35)((X(I,J),J=1,N),I=1,(NT+10))
35    FORMAT (11F11.4)
      WRITE (12,40)
40    FORMAT (//40X,"Z-COORDINATES"//)
      WRITE (12,35)((Z(I,J),J=1,N),I=1,(NT+10))
      WRITE (12,50)
50    FORMAT (//40X,"SIGMA VALUES"//)
      WRITE (12,35)((SIG(I,J),J=1,N),I=1,(NT+10))
      WRITE (12,60)
60    FORMAT (//40X,"THETA VALUES"//)
      WRITE (12,35)((THE(I,J),J=1,N),I=1,(NT+10))
75    ACCEPT "INPUT 1 FOR PLOT, ELSE 0 ",M
      ACCEPT "INPUT SCALE ",SC
      IF(M.EQ.1) CALL PLTSL(X,Z,THE,N,NT,HLENG,DEPTH,SC)
      CLOSE 12
      STOP
      END
```

```
      SUBROUTINE PLTSL(X,Z,THE,N,NT,HLENG,DEPTH,SC)
      DIMENSION X(21,11),Z(21,11),THE(21,11)
      CALL IN602 (1,"PASS.PLT")
      DO 6 J=1,N
      DO 6 I=1,(2*N-1)
      X(I,J)=SC*X(I,J)
    6 Z(I,J)=-SC*Z(I,J)
      CALL PLT602 (7.5,0.,3)
      CALL PLT602 (0.,0.,2)
      CALL PLT602 (0.,(-SC*DEPTH),2)
      CALL PLT602 ((SC*HLENG),(-SC*DEPTH),2)
      CALL PLT602 (0.,0.,2)
      DO 5 J=2,N
      K=N+1-J
      CALL PLT602 (X(K,J),(Z(K,J)),3)
      DO 5 I=(K+1),(NT+J-1)
    5 CALL PLT602 (X(I,J),(Z(I,J)),2)
      DO 3 I=2,(NT+N-2)
      K=N+1-I
      IF(I.GT.N) K=I-NT+1
      CALL PLT602 (X(I,K),(Z(I,K)),3)
      DO 3 J=(K+1),N
    3 CALL PLT602 (X(I,J),(Z(I,J)),2)
      CALL PLT602 (7.5,.25,3)
      CALL PLT602 (0.,.25,2)
      CALL PLT602 (X(N,1),(-.5*THE(N,1)+.25),2)
      DO 2 I=N,(NT+N-1)
      J=I-NT+1
    2 CALL PLT602 (X(I,J),(-.5*THE(I,J)+.25),2)
      CALL FIN602
      RETURN
      END
```

```
C                CYLINDER RIGID BODY
      DIMENSION X(21,11),Z(21,11),SIG(21,11),THE(21,11)
      OPEN 12,"ARRAYS.OUT",ATT="SQM"
      ACCEPT "INPUT PHI,GAMMA=  ",PHI,GAMMA
      TYPE "   PHI=",PHI,"   GAMMA=",GAMMA
      ACCEPT "INPUT DEPTH,LENGTH ",DEPTH,HLENG
      TYPE "DEPTH=",DEPTH,"   LENGTH=",HLENG
      ACCEPT "INPUT N ",N
      TYPE "N=",N
      GO=GAMMA
      ARC=.0174533
      PI=3.14159
      F1=ARC*PHI
      TF=TAN(F1)
      U1=PI/4-F1/2
   59 DO 58 J=1,N
      DO 58 I=1,21
      X(I,J)=0
      Z(I,J)=0
      SIG(I,J)=0
   58 THE(I,J)=0
      NT=N
      ACCEPT "INPUT DELTA,QBOT ",DELTA,QBOT
      TYPE "DELTA=",DELTA,"  QBOT=",QBOT
      DEL=ARC*DELTA
      DTHE=.5*(ATAN(SIN(SIN(DEL)/SIN(F1))/
    1 SQRT(1-(SIN(DEL)/SIN(F1))**2))+DEL)
      SIBOT=QBOT/(COS(DEL)+SQRT(COS(DEL)**2-COS(F1)**2))
      DO 80 J=1,N
      I=N+1-J
      F=(FLOAT(J)-1)/(N-1)
      X(I,J)=HLENG
      Z(I,J)=F*DEPTH
      SIG(I,J)=F*SIBOT
   80 THE(I,J)=DTHE
      IF(ABS(THE(N,1)).GT.U1) NT=N-1
      TYPE "THE,U1= ",THE(N,1),U1
      DO 90 J=2,N
      DO 90 I=(N+2-J),(NT+J-1)
      IF(I.EQ.(NT+J-1)) GO TO 10
      L=0
      TH1=THE(I,J-1)+U1
      TH2=THE(I-1,J)-U1
      SI1=SIG(I,J-1)
      SI2=SIG(I-1,J)
      V7=2*SIG(I-1,J)*SIG(I,J-1)
      U9=SIG(I-1,J)+SIG(I,J-1)
      V8=(THE(I,J-1)-THE(I-1,J))*TF
      V9=2*SIG(I-1,J)*SIG(I,J-1)*V8
      U6=2*TF*(SIG(I,J-1)*THE(I,J-1)+SIG(I-1,J)*THE(I-1,J))
    5 V1=TAN(TH1)
      V2=TAN(TH2)
      XI=V1*X(I,J-1)
      XJ=V2*X(I-1,J)
      V12=1/(V1-V2)
      X(I,J)=V12*(Z(I-1,J)-Z(I,J-1)+XI-XJ)
      Z(I,J)=Z(I-1,J)+(X(I,J)-X(I-1,J))*V2
      AA=-TF*(X(I,J)-X(I-1,J))+(Z(I,J)-Z(I-1,J))
      BB=TF*(X(I,J)-X(I,J-1))+(Z(I,J)-Z(I,J-1))
      U5=SIG(I,J-1)-SIG(I-1,J)
      IF(U9.EQ.0) GO TO 15
      SIG(I,J)=(V7+V9+GO*(SI1*AA+SI2*BB))/U9
      THE(I,J)=(U5+U6+GO*(BB-AA))/(2*TF*U9)
      GO TO 16
```

```
15    SIG(I,J)=GO*(AA+BB)/(2+TF*(THE(I-1,J)-THE(I,J-1)))
      THE(I,J)=(BB*(1+THE(I-1,J))-AA*(1-THE(I,J-1)))/(AA+BB)
16    IF(L.EQ.1) GO TO 20
      TH1=.5*(THE(I,J-1)+THE(I,J))+U1
      TH2=.5*(THE(I-1,J)+THE(I,J))-U1
      SI1=.5*(SIG(I,J-1)+SIG(I,J))
      SI2=.5*(SIG(I-1,J)+SIG(I,J))
      U6=2*TF*(SI1*THE(I,J-1)+SI2*THE(I-1,J))
      V7=SI1*SIG(I-1,J)+SI2*SIG(I,J-1)
      V9=2*SI1*SI2*V8
      U9=SI1+SI2
      L=1
      GO TO 5
10    Z(I,J)=0
      SIG(I,J)=0
      TH3=TAN(THE(I-1,J)-U1)
      KK=0
11    X(I,J)=X(I-1,J)-Z(I-1,J)/TH3
      AA=-TF*(X(I,J)-X(I-1,J))+(Z(I,J)-Z(I-1,J))
      U3=SIG(I,J)-SIG(I-1,J)-GO*AA
      THE(I,J)=U3/(2*SIG(I-1,J)*TF)+THE(I-1,J)
      TH3=TAN(.5*(THE(I,J)+THE(I-1,J))-U1)
      IF(KK.EQ.6) GO TO 20
      KK=KK+1
      GO TO 11
20    IF(J.EQ.N) TYPE "I,J,X,Z= ",I,J,X(I,J),Z(I,J)
90    CONTINUE
      SIZ=-QBOT*SIN(DEL)
      P=SIZ*PI*HLENG*DEPTH+GO*PI*HLENG**2*DEPTH
      FQ=P/(GO*DEPTH*PI*HLENG**2)
      TYPE "P=",P,"  FQ=",FQ
      ACCEPT "INPUT 1 FOR CHANGE OF DATA,ELSE 0 ",IJK
      IF(IJK.EQ.1) GO TO 59
      ACCEPT "INPUT 1 FOR PRINT OF DATA,ELSE 0 ",KJI
      IF(KJI.EQ.0) GO TO 75
      WRITE (12,24)
24    FORMAT (/37X,"CYLINDER RIGID BODY",/"PHI,GO,DEPTH,HLENG,QBOT,"
     1 ,"P,FQ,DELTA")
      WRITE (12,25) PHI,GO,DEPTH,HLENG,QBOT,P,FQ,DELTA
25    FORMAT (10F10.4)
      WRITE (12,30)
30    FORMAT (//40X,"X-COORDINATES"//)
      WRITE (12,35)((X(I,J),J=1,N),I=1,(NT+10))
35    FORMAT (11F11.4)
      WRITE (12,40)
40    FORMAT (//40X,"Z-COORDINATES"//)
      WRITE (12,35)((Z(I,J),J=1,N),I=1,(NT+10))
      WRITE (12,50)
50    FORMAT (//40X,"SIGMA VALUES"//)
      WRITE (12,35)((SIG(I,J),J=1,N),I=1,(NT+10))
      WRITE (12,60)
60    FORMAT (//40X,"THETA VALUES"//)
      WRITE (12,35)((THE(I,J),J=1,N),I=1,(NT+10))
75    ACCEPT "INPUT 1 FOR PLOT, ELSE 0 ",M
      ACCEPT "INPUT SCALE ",SC
      IF(M.EQ.1) CALL PLTSLF(X,Z,THE,N,NT,HLENG,DEPTH,SC)
      CLOSE 12
      STOP
      END
```

```
      SUBROUTINE PLTSLF(X,Z,THE,N,NT,HLENG,DEPTH,SC)
      DIMENSION X(21,11),Z(21,11),THE(21,11)
      CALL IN602 (1,"PASS.PLT")
      DO 6 J=1,N
      DO 6 I=1,(2*N-1)
      X(I,J)=SC*X(I,J)
    6 Z(I,J)=-SC*Z(I,J)
      CALL PLT602 (7.5,0.,3)
      CALL PLT602 (0.,0.,2)
      CALL PLT602 (0.,(-SC*DEPTH),2)
      CALL PLT602 ((SC*HLENG),(-SC*DEPTH),2)
      CALL PLT602 ((SC*HLENG),0.,2)
      DO 5 J=2,N
      K=N+1-J
      CALL PLT602 (X(K,J),(Z(K,J)),3)
      DO 5 I=(K+1),(NT+J-1)
    5 CALL PLT602 (X(I,J),(Z(I,J)),2)
      DO 3 I=2,(NT+N-2)
      K=N+1-I
      IF(I.GT.N) K=I-NT+1
      CALL PLT602 (X(I,K),(Z(I,K)),3)
      DO 3 J=(K+1),N
    3 CALL PLT602 (X(I,J),(Z(I,J)),2)
      CALL PLT602 (7.5,.25,3)
      CALL PLT602 ((X(N,1)),.25,2)
      CALL PLT602 (X(N,1),(-.5*THE(N,1)+.25),2)
      DO 2 I=N,(NT+N-1)
      J=I-NT+1
    2 CALL PLT602 (X(I,J),(-.5*THE(I,J)+.25),2)
      CALL FIN602
      RETURN
      END
```

APPENDIX B

SAMPLE PRINTOUT

CONE RIGID BODY

PHI,GO,DEPTH,HLENG,GDOT,P,FB,DELTA

42.0000 .0040 9.0000 1.5000 1.1700 14.1200 3.4259 -21.0000

X COORDINATES

.0000	.0000	.0000	.0000	.0000	.0000	.0000	.0000	.0000	.0000	1.5000
.0000	.0000	.0000	.0000	.0000	.0000	.0000	.0000	.0000	1.3500	2.1345
.0000	.0000	.0000	.0000	.0000	.0000	.0000	.0000	1.2000	1.7059	2.7953
.0000	.0000	.0000	.0000	.0000	.0000	.0000	1.0500	1.6077	2.6514	3.4842
.0000	.0000	.0000	.0000	.0000	.0000	.9000	1.6701	2.5092	3.3403	4.2003
.0000	.0000	.0000	.0000	.0000	.7500	1.5404	2.3073	3.2150	4.0707	4.9360
.0000	.0000	.0000	.0000	.0000	1.3900	2.2300	3.0077	3.7500	4.0127	5.6090
.0000	.0000	.0000	.4500	1.2550	2.1025	2.9655	3.8205	4.6827	5.5247	6.3500
.0000	.0000	.0000	1.1103	1.7610	2.0450	3.6045	4.5221	5.3293	6.1137	6.8730
.0000	.1500	.9976	1.6637	2.6707	3.4079	4.2472	4.9860	5.7107	6.4252	7.1320
.0000	.7465	1.6245	2.4725	3.1687	3.8097	4.5026	5.1621	5.8199	6.4760	7.1302
.0000	.0000	2.0315	2.8405	3.5817	4.3147	5.0212	5.7206	6.4008	7.0915	7.7701
.0000	.0000	.0000	3.0494	3.9702	4.6700	5.4666	6.1902	6.9027	7.6037	8.2960
.0000	.0000	.0000	.0000	4.1712	5.0016	5.6476	6.6209	7.3736	8.0772	8.8071
.0000	.0000	.0000	.0000	.0000	5.2254	6.1502	6.9476	7.7640	8.5051	9.2787
.0000	.0000	.0000	.0000	.0000	.0000	6.2042	7.2266	8.0502	8.7006	9.6055
.0000	.0000	.0000	.0000	.0000	.0000	.0000	7.3079	8.2094	9.1524	10.0237
.0000	.0000	.0000	.0000	.0000	.0000	.0000	.0000	8.3711	9.2944	10.2301
.0000	.0000	.0000	.0000	.0000	.0000	.0000	.0000	.0000	9.3901	10.2025
.0000	.0000	.0000	.0000	.0000	.0000	.0000	.0000	.0000	.0000	10.3720

Z COORDINATES

.0000	.0000	.0000	.0000	.0000	.0000	.0000	.0000	.0000	.0000	9.0000
.0000	.0000	.0000	.0000	.0000	.0000	.0000	.0000	.0000	8.1000	7.9493
.0000	.0000	.0000	.0000	.0000	.0000	.0000	.0000	7.2000	7.0501	6.9162
.0000	.0000	.0000	.0000	.0000	.0000	.0000	6.3000	6.1512	6.0231	5.9171
.0000	.0000	.0000	.0000	.0000	.0000	5.4000	5.2520	5.1296	5.0320	4.9021
.0000	.0000	.0000	.0000	.0000	4.5000	4.3545	4.2307	4.1544	4.1010	4.0776
.0000	.0000	.0000	.0000	3.6000	3.4573	3.3523	3.2866	3.2504	3.2641	3.2794
.0000	.0000	.0000	2.7000	2.5618	2.4745	2.4303	2.4475	2.4946	2.5723	2.6743
.0000	.0000	1.8000	1.6701	1.6164	1.6615	1.6993	1.8051	1.9377	2.0877	2.2559
.0000	.7600	.7707	.8173	.9303	1.0807	1.2712	1.4677	1.6701	1.8046	2.1064
.0000	.0000	.1534	.3747	.6258	.8737	1.1203	1.3659	1.6110	1.8555	2.0996
.0000	.0000	.0000	.2012	.3755	.6113	.8346	1.0662	1.2923	1.5242	1.7574
.0000	.0000	.0000	.0000	.2072	.3707	.5729	.7874	1.0006	1.2309	1.4619
.0000	.0000	.0000	.0000	.0000	.1679	.3211	.5163	.7266	.9449	1.1666
.0000	.0000	.0000	.0000	.0000	.0000	.1770	.3666	.4766	.6753	.8054
.0000	.0000	.0000	.0000	.0000	.0000	.0000	.1643	.2675	.4325	.6246
.0000	.0000	.0000	.0000	.0000	.0000	.0000	.0000	.1727	.2470	.3740
.0000	.0000	.0000	.0000	.0000	.0000	.0000	.0000	.0000	.1065	.2317
.0000	.0000	.0000	.0000	.0000	.0000	.0000	.0000	.0000	.0000	.2157
.0000	.0000	.0000	.0000	.0000	.0000	.0000	.0000	.0000	.0000	.0000

SIGMA VALUES

.0000	.0000	.0000	.0000	.0000	.0000	.0000	.0000	.0000	.0000	.7007
.0000	.0000	.0000	.0000	.0000	.0000	.0000	.0000	.0000	.7026	.7066
.0000	.0000	.0000	.0000	.0000	.0000	.0000	.0000	.6240	.0000	.6364
.0000	.0000	.0000	.0000	.0000	.0000	.0000	.5465	.5522	.5611	.5731
.0000	.0000	.0000	.0000	.0000	.0000	.4664	.4744	.4841	.4973	.5139

.0000	.0000	.0000	.0000	.0000	.3704	.3567	.4074	.4220	.4410	.4032
.0000	.0000	.0000	.0000	.3120	.3192	.3015	.3407	.3764	.3750	.4245
.0000	.0000	.0000	.2342	.2420	.2507	.2775	.3035	.3325	.3609	.4000
.0000	.0000	.1561	.1656	.1647	.2114	.2438	.2804	.3200	.3617	.4052
.0000	.0701	.0918	.1204	.1500	.2005	.2460	.2731	.3415	.3907	.4465
.0000	.0000	.0510	.1044	.1599	.2140	.2074	.3209	.3780	.4027	.4809
.0000	.0000	.0000	.0505	.0772	.1492	.2002	.2517	.3037	.3557	.4004
.0000	.0000	.0000	.0000	.0518	.0970	.1466	.1966	.2475	.2909	.3507
.0000	.0000	.0000	.0000	.0000	.0475	.0750	.1434	.1932	.2430	.2950
.0000	.0000	.0000	.0000	.0000	.0000	.0407	.071[illegible]	.1335	.1071	.2048
.0000	.0000	.0000	.0000	.0000	.0000	.0000	[illegible]	.0704	.1362	.1043
.0000	.0000	.0000	.0000	.0000	.0000	.0000	[illegible]	.0434	.0004	.1020
.0000	.0000	.0000	.0000	.0000	.0000	.0000	[illegible]	.0000	.0475	.0074
.0000	.0000	.0000	.0000	.0000	.0000	.0000	.0000	.0000	.0000	.0512
.0000	.0000	.0000	.0000	.0000	.0000	.0000	.0000	.0000	.0000	.0000

TIETA VALUES

.0000	.0000	.0000	.0000	.0000	.0000	.0000	.0000	.0000	.0000	-.6202
.0000	.0000	.0000	.0000	.0000	.0000	.0000	.0000	.0000	-.6202	-.5900
.0000	.0000	.0000	.0000	.0000	.0000	.0000	.0000	-.6202	-.5931	-.5665
.0000	.0000	.0000	.0000	.0000	.0000	.0000	-.6202	-.5092	-.5591	-.5300
.0000	.0000	.0000	.0000	.0000	.0000	-.6202	-.5042	-.5493	-.5160	.4040
.0000	.0000	.0000	.0000	.0000	.6202	-.5771	-.5358	.4970	-.4611	-.4203
.0000	.0000	.0000	.0000	-.6202	-.5667	-.5162	-.4079	-.4205	.3919	-.3600
.0000	.0000	.0000	-.6202	-.5477	-.4351	-.4287	-.3009	.3411	-.3002	-.2810
.0000	.0000	-.6202	-.5173	-.4274	-.3403	-.3077	-.2186	-.2307	.2156	-.1975
.0000	-.6202	-.4335	-.3007	-.2362	-.1935	-.1668	-.1487	-.1301	-.1267	-.1194
.6202	-.5130	-.0010	-.0070	-.0600	-.0020	-.0027	.0029	-.0001	-.0030	-.0005
.0000	.0000	-.3706	-.2009	-.1564	-.1263	-.1107	-.1013	-.0750	.0906	.0873
.0000	.0000	.0000	-.4615	-.2389	-.1866	-.1466	-.1250	.1131	-.1040	.0700
.0000	.0000	.0000	.0000	-.5246	-.2742	-.2046	-.1560	-.1040	-.1202	-.1105
.0000	.0000	.0000	.0000	.0000	-.0131	-.3364	.2473	-.1071	.1555	-.1364
.0000	.0000	.0000	.0000	.0000	.0000	-.6719	-.3774	-.2715	-.2027	-.1670
.0000	.0000	.0000	.0000	.0000	.0000	.0000	-.7303	-.4401	-.3072	-.2264
.0000	.0000	.0000	.0000	.0000	.0000	.0000	.0000	-.7790	-.5044	-.3405
.0000	.0000	.0000	.0000	.0000	.0000	.0000	.0000	.0000	-.8001	-.5057
.0000	.0000	.0000	.0000	.0000	.0000	.0000	.0000	.0000	.0000	.7024

REFERENCES

Adams, J. I. and D. C. Hayes (1967), "The Uplift Capacity of Shallow Foundations," Ontario Hydro Research Quarterly, Vol. 19, No. 1, First Quarter, pp. 1-13.

Baker, W. H. and R. L. Konder (1966), "Pullout Load Capacity of a Circular Earth Anchor Buried in Sand," National Academy of Sciences, Highway Research Record 108, pp. 1-10.

Balla, A. (1961), "The Resistance to Breaking-out of Mushroom Foundations for Pylons," Proceedings, Fifth International Conference on Soil Mechanics and Foundation Engineering, Paris, Vol. 1, pp. 569-576.

Bemben, S. W., M. Kupferman and E. H. Kalajian (1971), "The Vertical Holding Capacity of Marine Anchors in Sand and Clay Subjected to Static and Cyclic Loading," U.S. Naval Civil Engineering Laboratory Report No. CR 72 007.

Chen, W. F. (1975), Limit Analysis and Soil Plasticity, Elsevier Scientific Publishing Company, New York.

Das, B. M. and G. R. Seeley (1975), "Breakout Resistance of Shallow Horizontal Anchors," Journal of the Geotechnical Engineering Division, ASCE, Vol. 1, No. GT9, Technical Note, Proc. Paper 11538, pp. 999-1004.

Esquivel-Diaz, R. F. (1967), "Pullout Resistance of Deeply Buried Anchors in Sand," thesis presented to Duke University at Durham, S.C., in partial fulfillment of the requirements for the degree of Master of Science (available as Duke Soil Mechanics Series No. 8).

Harr, M. E. (1966), Foundations of Theoretical Soil Mechanics, McGraw-Hill, New York, N.Y., pp. 233-324.

Healy, K. A. (1971), "Pull-Out Resistance of Anchors Buried in Sand," Journal of the Soil Mechanics and Foundations Division, ASCE, Vol. 97, No. SM11, Technical Note, Proc. Paper 8511, pp. 1615-1622.

Karafiath, L. L. and E. A. Nowatzki (1978), Soil Mechanics for Off-Road Vehicle Engineering, Trans Tech Publications, Clausthal, West Germany, pp. 163-264.

Kovacs, W. D. and F. Y. Yokel (1979), "Soil and Rock Anchors for Mobile Homes--A State-of-the-Art Report," NBS Building Science Series 107, U.S. Department of Commerce, National Bureau of Standards, Washington, D.C.

Lee, I. K. and J. R. Herrington (1972), "A Theoretical Study of the Pressures Acting on a Rigid Wall by a Sloping Earth on Rock Fill," Geotechnique, Vol. 22, No. 1, pp. 1-26.

Nowatzki, E. A. and L. L. Karafiath (1981), "Plasticity Solutions for Upward Passive Earth Pressure," (submitted to Geotechnique for publication).

Rowe, P. W. and K. Peaker (1965), "Passive Earth Pressure Measurements," Geotechnique, Vol. 15, No. 1, pp. pp. 57-78.

Sokolovskii, V. V. (1960), Statics of Soil Media, 2nd ed., (translated from Russian by D. H. Jones and A. N. Schofield), Butterworths, London.

Sokolovskii, V. V. (1965), Statics of Granular Media, Pergamon Press, New York.

Sutherland, H. B. (1965), "Model Studies for Shaft Raising Through Cohesionless Soils," Proceedings, Sixth International Conference on Soil Mechanics and Foundation Engineering, Vol. II, Montreal, pp. 410-413.

Vesic, A. S. (1971), "Breakout Resistance of Objects Embedded in Ocean Bottom," Journal of the Soil Mechanics and Foundations Division, ASCE, Vol. 97, No. SM9, Proc. Paper 8372, pp. 1183-1205.